



## ORIGINAL ARTICLE

# Structural and electrical properties of polyvinyl alcohol (PVA):Methyl cellulose (MC) based solid polymer blend electrolytes inserted with sodium iodide (NaI) salt



Aziz M. Abdullah <sup>a</sup>, Shujahadeen B. Aziz <sup>b,c,\*</sup>, Salah R. Saeed <sup>a</sup>

<sup>a</sup> Department of Applied Physics, College of Medical and Applied Sciences, Charho University, Peshawa Street, Chamchamal, Sulaimani 46001, Iraq

<sup>b</sup> Hameed Majid Advanced Polymeric Materials Research Lab., Physics Department, College of Science, University of Sulaimani, Qlyasan Street, Sulaimani 46001, Kurdistan Regional Government, Iraq

<sup>c</sup> Department of Civil Engineering, College of Engineering, Komar University of Science and Technology, Sulaimani 46001, Kurdistan Regional Government, Iraq

Received 15 June 2021; accepted 10 August 2021

Available online 1 September 2021

## KEYWORDS

PVA and MC polymers;  
NaI salt;  
Polymer blending;  
FTIR, and XRD methods;  
Impedance spectroscopy  
study

**Abstract** This paper studies the structural and electrical properties of solid polymer blend electrolytes based on polyvinyl alcohol (PVA) and methylcellulose (MC) incorporated with sodium iodide (NaI). The polymer electrolyte films were assembled through a solution casting technique. The host matrix, which is doped with different NaI salt concentrations between 10 and 50 wt%, utilizes the most amorphous blend compositions (60 wt% Polyvinyl alcohol and 40 wt% methylcellulose). The structural behaviour of the electrolyte films was examined utilizing X-ray diffraction (XRD) and Fourier transformation infrared (FTIR) techniques. The semi crystalline nature of PVA:MC with inserted NaI was derived from the X-ray diffraction studies, while the XRD analysis suggests that the highest ion conductive sample displays the minimum crystalline nature. The interaction between polymer blends and inserted salt was conceived from the FTIR investigation. Shifting of peaks and variation in the intensity of FTIR bands was detected. To investigate the structural properties and calculate the degree of crystallinity of the films, the (XRD) technique was employed, while electrical impedance spectroscopy (EIS) was utilized for studying the conductivity of the samples. In order to comprehend all of the electrical properties of the ion-conducting systems, the EIS

\* Corresponding author at: Hameed Majid Advanced Polymeric Materials Research Lab., Physics Department, College of Science, University of Sulaimani, Qlyasan Street, Sulaimani 46001, Kurdistan Regional Government, Iraq.

E-mail address: [shujahadeenaziz@gmail.com](mailto:shujahadeenaziz@gmail.com) (S.B. Aziz).

Peer review under responsibility of King Saud University.



outcome of each electrolyte was matched with Equivalent Electrical Circuits (EEC)s. Ion transport parameters including mobility, carrier density and diffusion are well assessed for the samples and the dielectric properties were compared with the conductivity measurement. At lower frequencies, the dielectric constant was elevated and dielectric loss was detected. Loss tangent and electric modulus plots were used to study the relaxation nature of the samples. The highest ambient temperature conductivity of PVA loaded 50 wt% of NaI was determined to be  $1.53 \times 10^{-5}$  S/cm. The loss tangent relaxation peak shifts towards high-frequency side which indicates the decrease of relaxation time and faster ion dynamics.

© 2021 The Author(s). Published by Elsevier B.V. on behalf of King Saud University. This is an open access article under the CC BY-NC-ND license (<http://creativecommons.org/licenses/by-nc-nd/4.0/>).

## 1. Introduction

After realizing the disadvantages, directly and indirectly, related to the utilization of electrolyte materials in energy storage/conversion, such as batteries and electrochemical supercapacitors (ESs), and the need for suitable devices compatible with the advancements of new display technology and portable devices, researchers and industrial centers alike have attempted the search for natural, eco-friendly/non-toxic, abundant, non-expensive electrolytes. (Kim et al., ; Liu et al., 2017 Nov 15; Pan et al., 2019; Zhong et al., 2015). Over the last few decades, the focus on bio-based polymers (BBPs) is growing considerably as potential alternatives to conventional polymers. These materials would be used to solve global concerns. Generally, bio-based polymers refer to those obtained naturally from living organisms (Tanase et al., 2014). Polymers, due to their superior flexibility, good compatibility with electrodes, high dielectric strength, non-expensive and easy fabrication, and ionic conduction ability (since it was discovered by Wright in 1975 and the announcement of utilizing possibilities in batteries by Armand), have become a promising class of materials utilized as matrices and host polymers in the manufacturing of solid polymer electrolytes (SPEs) through the dissolution of salts in suitable high molecular weight polymers (Yao et al., 2019; Agrawal and Pandey, 2008; Di Noto et al., 2011). Researchers are committed to developing polymer electrolytes with excellent conductivity for application as separators in electrochemical devices, as ionic conductivity is considered the most significant characteristic of SPEs (Wang et al., 2016). In polymer electrolytes, however, the amorphous phase rather than the crystalline phase dominates ionic conduction. Non-toxicity, biodegradability, and sustainability are characteristics of natural polymers. Based on their synthesis and origin of source, BBPs can be classified into three main categories. First, those are extracted directly from the biomass, for example, starch, cellulose, chitosan, and alginates. This category is the most abundant and a significant resource of bio-based polymers. Secondly, polymers from bio-derived monomers are synthesized. Third, some polymers are derived from microorganisms/bacteria (Malhotra et al., 2015).

It is worth noting that biopolymers, including polyvinyl alcohol (PVA), methylcellulose (MC), starch, dextran, gum, and carrageenan, are considered a strong alternative to non-biodegradable synthetic polymers. Their electrochemical stability and their ability to form a stable film can be regarded as their most impressive characteristics to employ them in electrochemical devices, such as batteries, capacitors, and solar cells since these properties are decisive (Saito et al., 2017;

Ngai et al., 2016; Zeiger et al., 2016). Poly (vinyl alcohol) (PVA) is a water-soluble synthetic polymer that is known for its resistance to organic solvents. It is a partially crystalline polymer. The crystalline phase consists of plate-like single crystals (lamellae), 10–20 nm thick, that are bound to each other by disordered polymer chains and form an amorphous polymer phase. (Tretinnikov and Zagorskaya, 2012)

PVA is widely used and accepted as a host polymer, mainly due to the abundance (low cost), its good film-forming, high flexibility with superior chemicals and the thermal stability of the materials, as well as the greater extent of polar hydroxyl groups and its high chain flexibility which aids the salt-solvation process (Polu and Kumar, 2013; BalajiBhargav et al., 2007; Rani et al., 2020). The ability of PVA to form electrolytes is associated with its hydrophilic properties and several hydroxyl groups attached to methylene carbons (CH<sub>2</sub>-CH) on the PVA backbone (Remiš et al., 2021). Several investigations have been carried out on blending PVA with other biopolymers. It was observed that the addition of PVA could improve the film's flexibility and wettability. (Gao et al., 2014). Rani et al. (Rani et al., 2021) prepared Polyvinyl alcohol (PVA)/Chitosan (CS)/graphite oxide (GO)/ nickel oxide (NiO) nanocomposites using the solution casting technique. The author showed that the addition of both nanofillers to the PVA/CS blend enhanced the thermal stability of the nanocomposites by the interaction between the OH groups of the polymers and the nano-fillers. Most PVA properties depend on molecular weight and hydrolyzation (Baker et al., 2012). The execution of earlier studies has shown that the blending of two polymers is an effective method to modify the polymer properties and obtain specific unique characteristics otherwise impossible to be achieved using single polymers in order to avoid inherent limitations of neat polymers. Thus, instead of using a single polymer to produce SPEs, the blending of two or more different polymers can improve mechanical properties, thermal stability, and the availability of ion hopping sites (Park and Park, 2001; Zhu et al., ; Rebia et al., 2018). Therefore, blending PVA with other polymers which have similar solubility parameters can improve blend material performance, which is owed to the formation of strong hydrogen bonds instead of weak van der Waals interaction (Abdullah Zainab Waheed, 2019). In contrast, methylcellulose (MC) contains numerous hydrophilic carboxyl groups and a hydrophobic polysaccharide backbone. It has been used to make solid biopolymer electrolytes as a polymer host. The lone pair of electrons of the MC at its oxygen atoms easily interacts with the cation of the salt to form polymer electrolytes based on MC (Park and Park, 2001). Additionally, MC is an

amorphous polymer possessing a relatively high glass transition temperature. It has an excellent ability to reduce the degree of crystallinity of the used polymer in the blending process (Sugantha Kumari et al., 2012). Polymer blend based on MC and PVA is easy to prepare since they are both water soluble, and they are miscible with each other.

The availability and abundance at a lower cost than lithium reflect the main advantage of using sodium metal ions in the electrolyte preparation. Another advantage is the softness of the material, which makes it easier to achieve good contact with other components in the electrochemical device (Tănase et al., 2015; Abiddin and Ahmad, 2015). In the present study, PVA and MC were utilized in an excellent blending process by incorporating sodium iodide (NaI). This work intends to derive films with a large proportion of the amorphous phase with far better conductivity than crystalline. Electrochemical impedance spectroscopy (EIS), X-ray diffraction (XRD) and FTIR were used to study the prepared PVA:MC systems incorporated with various NaI amounts.

From the fundamental and industrial points of view, the synthesis and development of biopolymers are vitally important. Studies of BBPs attempt to develop new systems of polymer electrolytes for possible applications at a large scale, including electrochemical devices. The current study's findings are critical for comprehending the fundamental links between DC conductivity and dielectric characteristics. In addition, the  $\tan \delta$  and electric modulus studies provide insight into the ion conduction mechanism in polymer electrolytes as a function of salt concentrations, expecting the system's possible applications. Singh et al. (xxxx) synthesized SPEs based on PVA/ ionic liquid (IL)/ 1-Butyl-2, 3-dimethylimidazolium tetrafluoroborate [BDMITFB] and characterized the films using AC impedance spectroscopy technique. The authors showed that the mobility, number density of charge carriers, dielectric constant, and DC conductivity considerably increased for the higher IL (20 and 25 wt%) loaded films. The aim of this work is to obtain high ionic conductivity and stabilized electrochemical properties from the PVA:MC blend polymer electrolytes by the dissolution of NaI salt. The prime novelty of this study is to progress and characterize the prepared blend polymer electrolytes with improved structural and electrical properties.

## 2. Materials and methods

### 2.1. Materials

PVA (Mw 89,000–98,000, 99+ % hydrolyzed), Methyl cellulose (MC) (M0262 Sigma-Aldrich) and Sodium Iodide (NaI) (Sigma-Aldrich, molecular weight g/mol) were purchased from Sigma-Aldrich Kuala Lumpur, Malaysia) and they were used as received without further purification.

### 2.2. Polymer blend electrolyte preparation

The first solution set was prepared using a solution cast technique by dissolving 0.4 g of MC in room temperature and 0.6 g of PVA (at 90 °C) in (40 ml) distilled water, separately. The solutions were stirred continuously with the magnetic stirrer for 24 h until an identical aqueous solution was obtained. Next, the PVA solution was cooled down to the ambient

temperature and mixed with MC. The process is finalized by stirring the blending of PVA:MC until clear solutions are attained. Finally, the sodium salt was used to prepare ion-conducting polymer electrolytes. Various quantities of NaI salt (10, 20, 30, 40, and 50 wt%) were added separately to the PVA MC solution, followed by continuous stirring for 24 h until clear solutions were obtained. The solutions were put into several plastic Petri dishes (8 cm in diameter) and then rested to allow the formation of a dry film exempt from solvent at ambient temperature. Then, flexible films with a thickness around 0.026 mm were formed.

The blend systems of PVA:MC doped with various amounts of NaI were coded as PVMCNI, PVMCNI1, PVMCNI2, PVMCNI3, PVMCNI4 and PVMCNI5, which corresponded to 0, 10, 20, 30, 40, and 50 wt% of NaI, respectively.

The composition of the prepared films are illustrated in Table 1.

### 2.3. XRD and FTIR characterization

The XRD patterns of the pure and composition polymer films have been recorded using X'Pert Pro diffractometer (PanAnalytical) with a  $\text{CuK}\alpha$  radiation source ( $\lambda = 1.54 \text{ \AA}$ ), in the  $2\theta$  range ( $10^\circ$ – $70^\circ$ ), to report the information concerning the crystal structure of the prepared films. To know the nature of the interaction between the components of the composites, a Perkin Elmer FTIR spectrometer was used with running in the area between  $400$  and  $4000 \text{ cm}^{-1}$  with a resolution of  $2 \text{ cm}^{-1}$ .

### 2.4. Impedance and dielectric properties

The impedance analysis is an appropriate method to study electrochemical properties and dynamics of ions through the operation of an LCR meter (HIOKI 3531 Z Hi-tester Japan) linked to a computer. The procedure requires preparing small disc-shaped films with a diameter of around 2.0 cm and inserting them between two stainless steel electrodes with spring pressure to make proper contact. By connecting the cell with a computer program, the imaginary ( $Z''$ ) and real ( $Z'$ ) parts of the complex impedance ( $Z^*$ ) data were measured. In addition, the Nyquist plot intercept with the axis of  $Z'$  shows and determines the resultant bulk resistance ( $R_b$ ), which is critical to determine the electrolytes' conductivity. From Eq. (1), the electrical characteristics of electrolytes can be estimated by measuring the ionic conductivity ( $\sigma$ ). The calculation also includes  $R_b$ ,  $t$ , and  $A$ , respectively, as charge resistance, thickness and surface area (Daniel et al., 2018).

**Table 1** Composition of PVA:MC:NaI-based solid polymer electrolytes.

Designation	PVA:MC (g)	NaI Wt. %	NaI (g)
PVMCNI0	(0.6: 0.4)	0.0	0.000
PVMCNI1	(0.6: 0.4)	10	0.111
PVMCNI2	(0.6: 0.4)	20	0.250
PVMCNI3	(0.6: 0.4)	30	0.428
PVMCNI4	(0.6: 0.4)	40	0.666
PVMCNI5	(0.6: 0.4)	50	1.000

$$\sigma_{dc} = \left( \frac{1}{R_b} \right) \times \left( \frac{l}{A} \right) \quad (1)$$

The dielectric study of each electrolyte is beneficial for further understanding of the conductivity behaviour and the polarization effects. The dielectric constant,  $\epsilon_r$ , is the number of charges stored. In contrast, the dielectric loss,  $\epsilon_i$  is the energy loss during the movement of ions within the electrolytes. Both dielectric parameters can be expressed using the following equations (Ibrahim et al., 2012).

$$\epsilon_r = \left[ \frac{Z_i}{\omega C_0 (Z_r^2 + Z_i^2)} \right] \quad (2)$$

$$\epsilon_i = \left[ \frac{Z_r}{\omega C_0 (Z_r^2 + Z_i^2)} \right] \quad (3)$$

$$\tan \delta = \frac{\epsilon_i}{\epsilon_r} \quad (4)$$

where,  $C_0$  refers to the usual meaning vacuum capacitance, and it is equal to  $\epsilon_0 A/t$ ; where  $\epsilon_0$  is the free space permittivity of  $8.85 \times 10^{-14} \text{F/cm}$ ,  $\omega$  is the angular frequency ( $\omega = 2\pi f$ ), and  $f$  is the applied field frequency. Eqs. (4) and (5) were used

for the real ( $M_r$ ) and imaginary ( $M_i$ ) parts of the electrical modulus, respectively (Aziz et al., 2019).

$$M_r = \omega C_0 Z_i \quad (5)$$

$$M_i = \omega C_0 Z_r \quad (6)$$

### 3. Results and discussion

#### 3.1. XRD analysis

Early studies showed that the XRD spectrum of pure PVA possesses various peaks at  $2\theta = 19.42^\circ$ , which is a typical sharp peak attributed to (101) plane. Also, there is a broad diffraction peak at  $2\theta = 41.31^\circ$  which is attributed to the (111) plane and indicates the semi-crystalline nature within the PVA structure (Jiang et al., 2015). The XRD diffraction patterns of pure PVA and pure MC and their blended films are presented in Fig. 1(a-c).

Reddy et al. (Reddy et al., 2020) prepared PVA/ cadmium sulphide nanoparticles (CdS) via solution casting technique. The authors observed that there was a decrease in the intensity

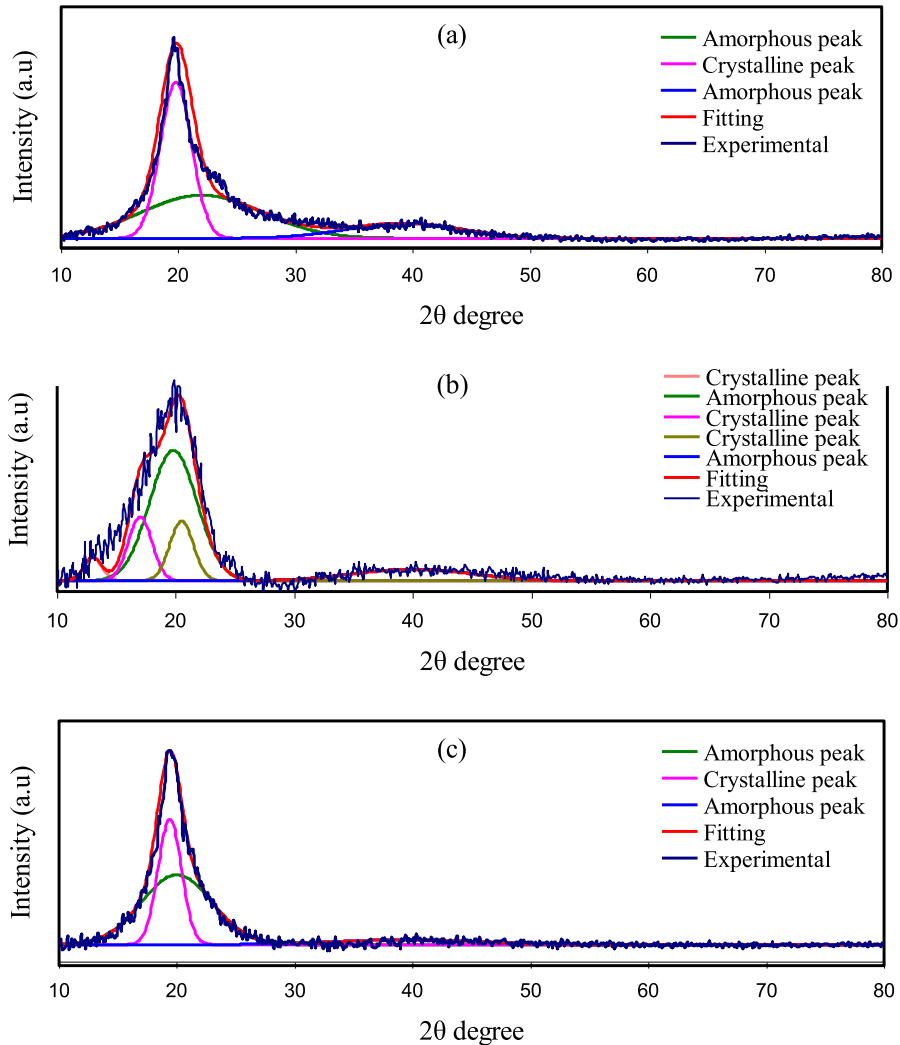


Fig. 1 XRD pattern of (a) pure PVA film, (b) pure MC, and (c) PVA: MC blend (60:40) films.

of the diffraction peaks with loading nanofiller concentration. They mentioned that this decrement might be due to substantial interaction between PVA chains and CdS nanoparticles. Reddy et al. (Reddy et al., 2019) in another study fabricated PVA/zinc sulphide nanoparticle (ZnS) nanocomposite films and studied the structure of the films using XRD method. In their study showed that the crystallinity of PVA considerably decreased with increasing ZnS nanoparticles.

The XRD pattern of the neat MC is also shown in Fig. 1(b). In the earlier investigations, pure MC exhibited broad humps and multiple weak peaks centred at  $2\theta = 13^\circ$ ,  $17^\circ$  and  $20^\circ$  (Saeed and Abdullah, 2020). Fig. 1(c) shows that the intensity of the XRD spectrum in the PVA main peak region is gradually reduced and extended by the addition of MC. This could be attributed to the disruption of the crystalline phase of PVA and the disturbance of the ordered arrangements of the PVA chains.

Furthermore, the molecular chain packing rearrangement has occurred, and the distorted structure appears after blending (Senna et al., 2018). This phenomenon is due to the significant hydrogen bonding interaction between PVA, and MC molecules, signifying that the fractional crystallinity of PVA has shrunk, which can be taken as evidence for the increase of amorphous state and good miscibility between the PVA and MC polymers (Kotobuki, 2020). It is generally acknowledged that hydrogen bonding occurs when electron-deficient hydrogen interacts with an area of high electron density. As an intermolecular interaction, hydrogen bondings (H-bonding), in fact, are expressed as X-H...Y, where X and Y are electronegative elements and Y has one or more lone electron pairs, i.e., X and Y are F, O, and N atoms (Singh et al., 2018). Therefore, the complexation between the PVA and MC polymers is well confirmed by our XRD analyses.

The XRD pattern of pure NaI is demonstrating in Fig. 2. It can be seen from Fig. 2 that the crystalline peaks of pure NaI salt are detected at  $2\theta = 18.5^\circ$ ,  $20.6^\circ$ ,  $23.67^\circ$ ,  $29.74^\circ$ ,  $32.69^\circ$ ,  $37.84^\circ$ ,  $39.12^\circ$ , and  $46.5^\circ$ ,  $56.75^\circ$ ,  $64.27^\circ$ ,  $71.24^\circ$ ,  $76.33^\circ$ . In the NaI complexed PVA-MC films, the diffraction peaks have

disappeared and changed to smaller diffraction peaks compared to the pure NaI pattern. Also, the degree of polymers crystallinity has found to be reduced with inclusion of the NaI salt. The absence of sharp peaks for high NaI ratios indicated that the amorphous phase is dominating, which is providing a clear suggestion of blend polymers-salt complexation. Fig. 3(a-d) shows the X-ray diffraction patterns of the PVA:MC blend incorporated with various concentrations of the NaI salt from (10–50) % in steps of 10. Fig. 3(a) shows a broad peak at  $19.42^\circ$  attributed to the PVA/MC blend polymer. It may be noted that with increasing NaI concentration, the intensity of the main peak PVA:MC polymer blends progressively decreases and the peak broadness increases, indicating the presence of molecular interactions between the polymer's functional groups and  $\text{Na}^+$  cations (Rani et al., 2014). Clearly, the peaks for the NaI disappear within the electrolyte spectrum. It is noteworthy to mention the increase in background noise indicating the enhancement in the amorphous phase, or in other words, the crystallinity of the sample gets reduced to a lesser degree (based on Bragg's law), which may be due to the cation coordination with an electron-rich group of PVA:MC host polymer (Arya and Sharma, 2017). The absence of any sharp peaks related to pure sodium iodide (NaI) confirms the complete dissolution of NaI salt within the polymeric matrix.

To measure the degree of crystallinity ( $X_c$ ) of pure and electrolyte films, Origin 8 software has been used to estimate the amorphous areas and the areas of crystalline peaks. The percent relative crystallinities ( $X_c$ ) were calculated from the following relationship and shown in Table 2 (Brza et al., 2021).

$$X_c = \left[ \frac{A_c}{A_c + A_a} \right] \times 100\% \quad (7)$$

where,  $A_c$  and  $A_a$  refer to the areas of crystalline and amorphous peaks, respectively. It worth noting that when additional NaI salt is added, the degree of crystallinity is suppressed more effectively, which may be attributed to the disruption of the polymer crystalline phase (Arya and

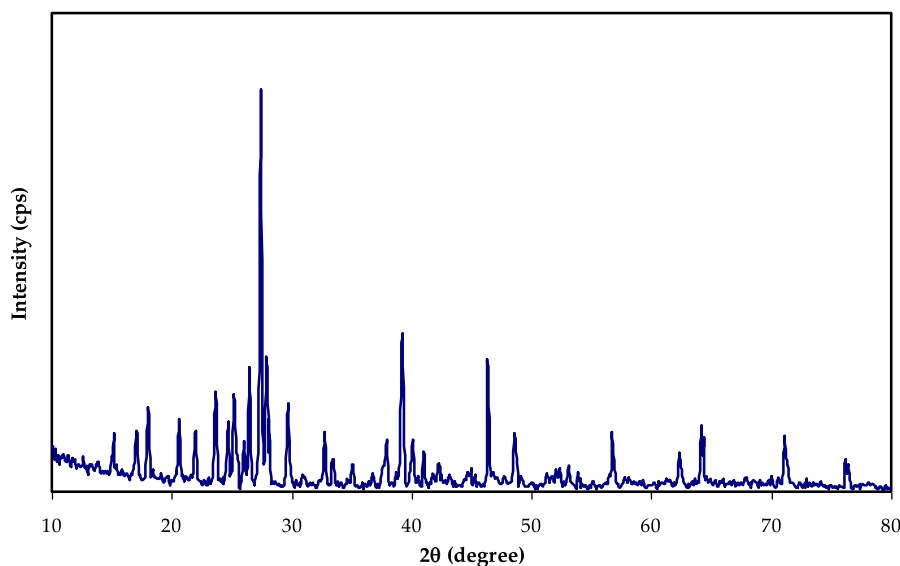
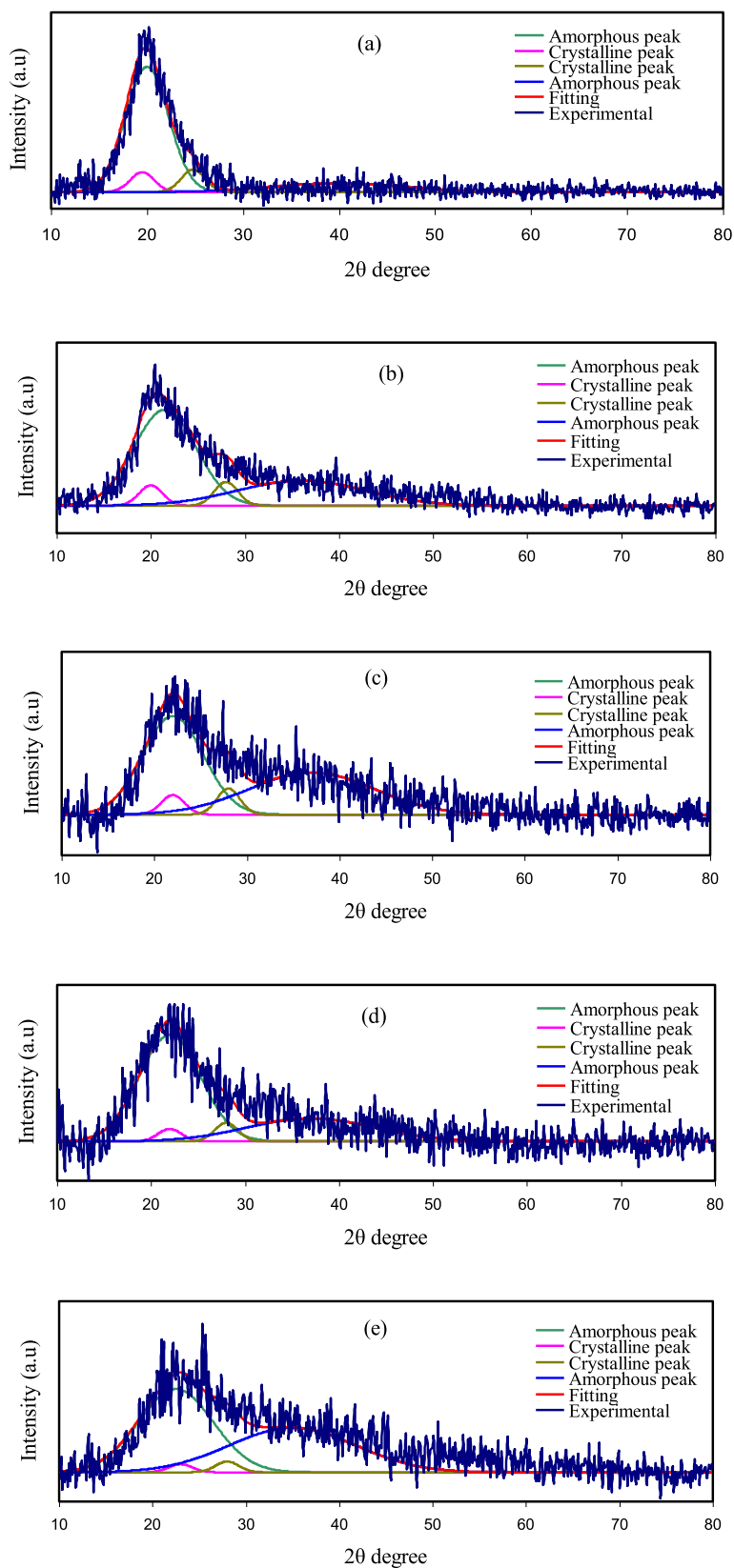


Fig. 2 XRD pattern of pure NaI.



**Fig. 3** X-ray diffraction (XRD) spectra for (a) PVMCNI1, (b) PVMCNI2, (c) PVMCNI3, (d) PVMCNI4, and (e) PVMCNI5 electrolyte films.

**Table 2** The  $X_c$  using deconvoluted XRD examination.

Electrolytes	Degree of crystallinity
Pure PVA	41.68
Pure MC	30.67
PVA:MC blend	34.61
PVMCNI1	13.38
PVMCNI2	10.15
PVMCNI3	8.53
PVMCNI4	7.14
PVMCNI5	3.55

Sharma, 2017). The degree of crystallinity achieved in this study for neat PVA (41.68) is comparable to that reported by other researchers in the literature (Jaipal Reddy and Chu, 2002).

### 3.2. FTIR study

The Fourier transform infrared (FTIR) spectroscopy has been utilized to investigate the compositional, structural and possible interactions between the functional groups of PVA and MC polymers in PVA:MC polymer blend films and to investigate the interaction between the blended (PVA:MC) host polymer with NaI salt, through the observed changes in the position, shape, and intensity of the IR transmittance bands in the wavenumber range from 400 to 4000  $\text{cm}^{-1}$ . The vibrational frequency peaks of OH, C-O, C-H,  $\text{CH}_2$ , and C=O

can be used as the characteristic bands for polymers PVA and MC (Olewnik-Kruszkowska, et al., 2093). Their changing considered as evidence of the compatibility in the blend polymer, which has an essential role in the amorphous phase enhancement inside the PVA:MC blend system. Fig. 4 shows the FTIR spectra of neat MC, PVA and their blending. Table 3 lists the FTIR peaks and their assignments for the pure polymers. As seen in Fig. 4, in the PVA:MC system, the OH bands become broader with less intensity, suggesting a decrease of PVA crystallinity. This observation is well consistent with the findings of the study of XRD. In the FTIR spectrum, the major peaks of pure PVA are comparable to the position of the characteristic bands mentioned in the previous works and earlier investigations (Rozali et al., 2012). The shift in the O-H peak position and intensity indicates that hydrogen bonds between the PVA hydrogen atoms and the MC oxygen atom are formed and, hence, PVA blending with MC. On blending with MC, the crystalline peak in the PVA structure corresponded to the C-O stretching mode is broadened at about 1061  $\text{cm}^{-1}$ , and its intensity is also reduced (Negim, 2014). In addition, the absorption band intensity at 847  $\text{cm}^{-1}$ , which corresponds to the C-C stretching of (PVA), decreases with MC incorporation within the blend.

In contrast, the peak is absent in the pure MC film spectrum. This implies that the presence of physical blends and chemical interactions produces modifications to typical peaks of the spectrum when two or more polymers are blended. These observations show that between PVA and MC, there is good miscibility.

Fig. 5 shows the group frequencies of NaI at 560, 720, 890, 1014, 1176, 1603, 1620, 1742, 2021 and 3208  $\text{cm}^{-1}$ . In the

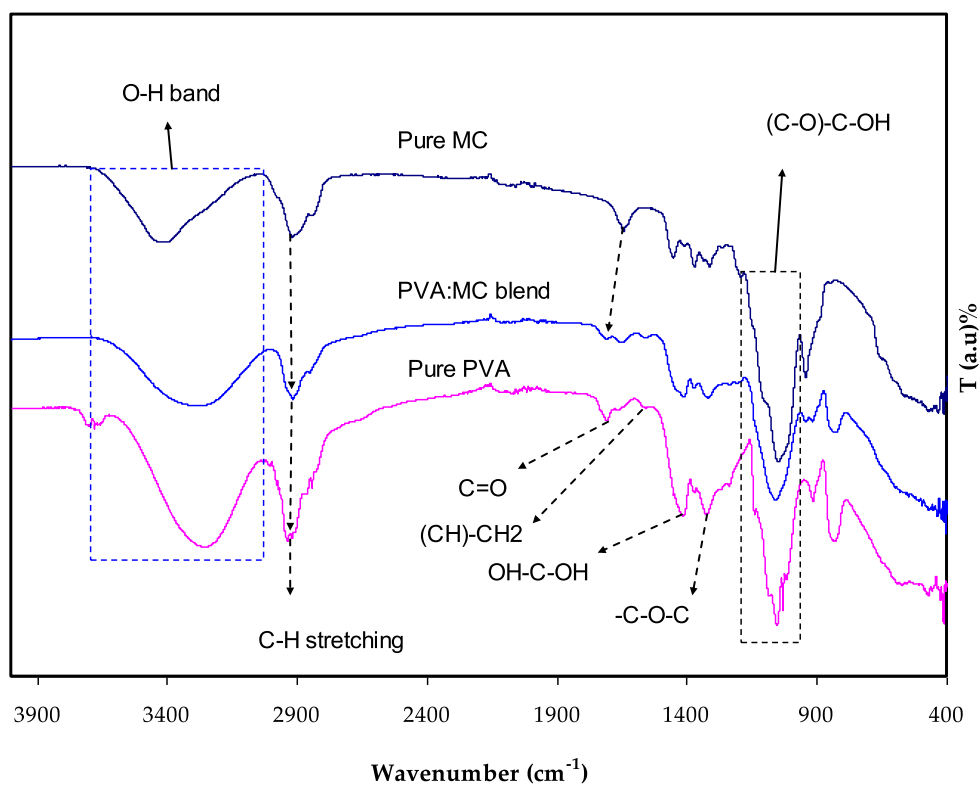


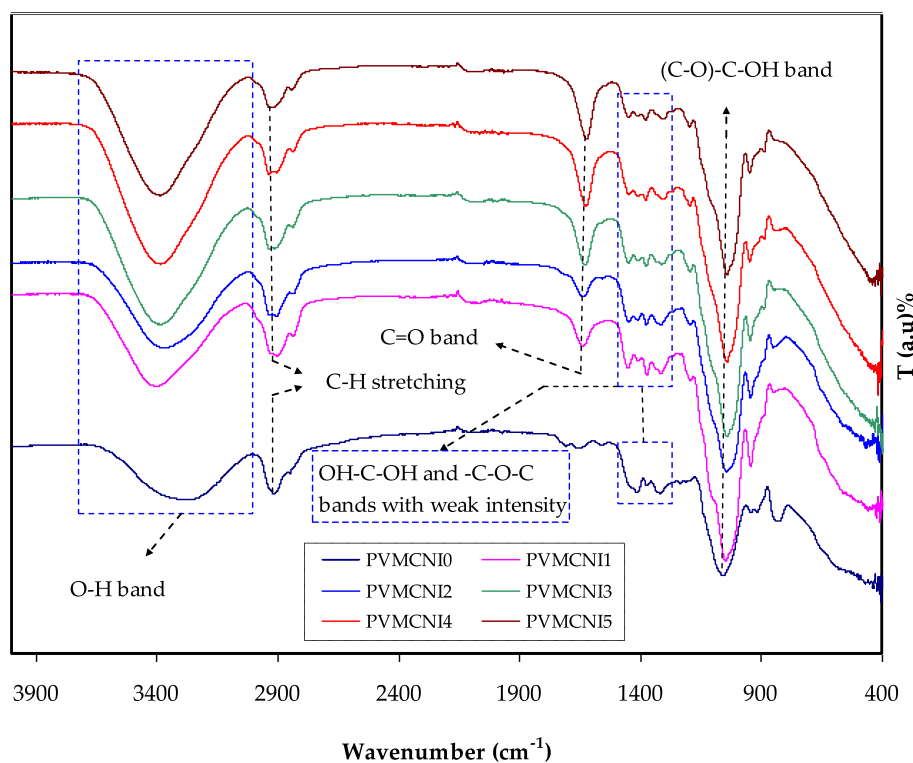
**Fig. 4** FTIR spectra for pure PVA, pure MC, PVA:MC (0.6:0.4) blend.

**Table 3** The FTIR results of pure (PVA), pure MC and blended PVA:MC.

Wavenumber (cm <sup>-1</sup> )			Vibrational modes
Pure PVA	Pure MC	PVMCNI0	
3283	3424	3259	O-H stretching
2910	2920	2937	C-H stretching
1712	–	1709	C = O
1553	–	1559	(C-H)-CH <sub>2</sub>
1416	1410	1414	OH-C-OH
1320	1315	1331	-C-O-C
1061	1050	1054	(C-O)-C-OH

wavenumber range between 400 and 4000 cm<sup>-1</sup>, the FTIR spectra of blended PVA:MC polymer mixed with different wt.% ratios of NaI in are shown in Fig. 5. The interaction happens by integrating salt into the polymer matrix. Between the salt and host polymers matrix, complex nature takes place. Singh and Saroj (Singh and Saroj, 2020). prepared plasticized polymer blend electrolytes based on PVA- polyvinyl pyrrolidone (PVP)-polyethylene glycol (PEG)-NaI- SiO<sub>2</sub>. Through the FTIR results the authors showed the interaction and complexation between SiO<sub>2</sub> nano-particles and the functional groups of the polymer blend electrolytes. When combined with PVA:MC, sodium iodide peaks are lost. The removal of these peaks confirms the macromolecular salt complexation. The interaction between PVA and NaI was therefore validated by FTIR spectroscopy and their complex formation. Table 4 reveals that the hydroxyl group (-OH) of blended PVA:MC

is greatly affected by the salt (NaI), where it was established to change the band after incorporation with NaI, and this result is agreed with previous studies (OmedGh. Abdullah, Shujahadeen B. Aziz, Mariwan A. Rasheed, Structural and optical characterization of PVA:KMnO<sub>4</sub> based solid polymer electrolyte, Results in Physics, Volume 6, ,2016) Because of the complex formation between the host polymer and added (NaI) salt, the change in the absorption frequency of the hydroxyl group (-OH). The C = O stretching of carboxyl is assigned to the stretching absorption band at 1709 cm<sup>-1</sup>. Carboxyls in the films are thought to mostly form intra- or inter-molecular hydrogen bonding with hydroxyl groups or other carboxyl groups (Choo et al., 2016 Jul 29). The complex building process between the functional groups of the host polymer and salt cations is implied by the apparent drop in transmittance intensity and band shifting. The vibration of the polar groups can be decreased as a result of the electrostatic interaction between salt cations and the functional groups (Negim, 2014). When comparing the spectrum of a complexed electrolyte to a pristine blended sample and NaI, the following alterations in the spectral characteristics were observed. In complexed films, the strong absorption peak of NaI salt at 1620 cm<sup>-1</sup> is shifted to 1625 cm<sup>-1</sup>. All these alterations in the FTIR spectrum provide clear evidence of PVA:MC complexation with NaI. The reduction in the intensity of the transmittance peak often signifies that the amount of the functional group (per unit volume) related to the molecular bond increases, while shifting in peak position generally signifies that the state of hybridization or electron distribution has changed in the molecular bond (OmedGh. Abdullah, Shujahadeen B. Aziz, Mariwan A. Rasheed, Structural and optical

**Fig. 5** FTIR spectra of pure PVA-MC blend (0.6:0.4), and PVA: MC: NaI polymer electrolytes for 10, 20, 30, 40, and 50 wt% systems.

**Table 4** The FTIR results of blended PVA:MC and NaI doped electrolytes.

Vibrational modes	Wavenumber (cm <sup>-1</sup> )					
	PVMCN10	PVMCN11	PVMCN12	PVMCN13	PVMCN14	PVMCN15
O-H stretching	3283	3405	3386	3386	3386	3397
C-H stretching	2910	2904	2905	2936	2938	2940
C = O	1712	–	–	–	–	–
(C-H)-CH <sub>2</sub>	1553	–	–	–	–	–
OH-C-OH	1416	1412	1412	1412	1412	1413
-C-O-C	1321	1315.9	1316	1314	1312	1312
(C-O)-C-OH	1061	1050	1046	1046	1045.5	1045

characterization of PVA:KMnO<sub>4</sub> based solid polymer electrolyte, Results in Physics, Volume 6, ,2016). Another interesting finding, induced by strong hydrogen bonds of intra and inter-type, is the formation of high-intensity bands of 1051 cm<sup>-1</sup> in PVA:MC:NaI electrolytes (Aziz, 2020). The C–O–C stretching vibration peak of pure PVA, based on previous studies (Fan, 2019), splits into three peaks at 1086, 1055, and 1032 cm<sup>-1</sup>

### 3.3. Electrical impedance spectroscopy (EIS)

Fig. 6(a-e) shows the complex impedance planes (i.e., Z'' vs Z') of the PVA:MC blend samples incorporated with different NaI ratios. Starting from the origin, the Nyquist plots consist of only small initial parts of semicircle at 10 and 20 wt% of NaI. In contrast, at 30 to 50 wt%, the semicircle and inclined tail at varied angles to the real axis were seen. There is evidence that high-frequency response provides information on the electrolyte characteristics, including bulk resistance and long-range ordering. On the other hand, the electrode/electrolyte interface can be characterized by low-frequency responses. The electrical behaviour of blended electrolyte films appears to be altered by adding salt to a blend polymer matrix.

The semicircle shows the bulk response of the sample at high frequencies, whilst the abrupt rise at low frequencies may be traced back to the double-layer charges accumulated at the solid polymer electrolyte/electrode interfaces. Collectively, this behaviour may be explained by the fact that the capacitor's impedance increases dramatically at lower frequencies ( $X_C = 1/2\pi fC$ ), implying that the resistor receives the majority of the current, causing its attributes to be dominated. However, at extremely high frequencies, the capacitor's impedance decreases to where the resistor is effectively shorted out, resulting in zero net impedance (Aziz et al., 2018). The decreasing semicircles at high frequency, specifying low resistance of the bulk resistance ( $R_b$ ), is displayed in the intercept of the arc with the  $Z_r$  axis and essentially vanishes at about 50 wt %. Within the impedance plot, the disappearing semicircular region at high frequency allows the conclusion that the total conductivity implies dominating ionic conduction of the whole conductivity at elevated salt concentration (Wani and Rafiuddin, 2018). As depicted in Fig. 6, a rise in salt concentration is followed by a decline in bulk resistance. The evaluation of the data shows that the value of  $R_b$  can be assessed from the intersection of the semicircle with the real axis ( $Z_r$ ) (Aziz, 2020). Eq. (1) was used to determine the DC conductivity of the films, and their values are exhibited in Table 5.

An increase in salt concentration will result in increased DC conductivity. Consequently, two distinct zones within the plots can be identified, one corresponding to electrode polarization in low-frequency ranges and the other to bulk material characteristics in high-frequency ranges (Aziz et al., 2020). The involvement of ionic conduction from bulk material gives rise to electrical processes within the material, indicated by the existence of the semicircle. The off-centred shape of the semicircles represents the non-Debye type relaxation process. In contrast, the low frequency restrained arc corresponds to the double-layer capacitance effect due to the ion's blocking at the end of the stainless-steel blocking electrodes. As a result, the movement of the charges is strictly restrained within a limited volume of the matter. Therefore, a polarization phenomenon happens, or the electrical charges within the respective material are completely diffused. Diffusion is therefore likely to occur, and a DC conductivity,  $\sigma_{dc}$ , develops (Aziz et al., 2017).

From a physics viewpoint, the dissipative part of the dielectric response is attributable to resistance. In contrast, the storage part of the dielectric material is shown by a capacitance (Aziz et al., 2019). The semicircle is produced at high by the parallel combination of bulk resistance ( $R_b$ ) and bulk capacitance induced by ion migration and static (immobile) polymer chains. The sharp increase at lower frequencies, on the other hand, is due to polarization at the electrode/electrolyte interface region (Basha and Rao, 2018, 2018.). At lower frequencies, mobile charges possess enough time to move under the influence of the applied external electrical field, causing the massing of charges at the polymer electrode interface. Once the salt is introduced to the polymer host, the decline in the curve shifts to the lower impedance value, suggesting lower bulk resistance and hence improved ionic conductivity. Furthermore, it is known that the complex impedance is dominated by the ionic conductivity in cases where the phase angle nears zero (Aziz et al., 2019).

The calculated ion transport parameters value of mobility ( $\mu$ ), number density of carrier ( $n$ ), and diffusion coefficient ( $D$ ) are also presenting in Table 5. All the values have found to be optimum for a highest conducting sample. The value of  $D$  increases when the amount of salt is increased from 30 to 50 wt% and a similar tendency is also seen for  $\mu$ . The increases in  $D$  and  $\mu$  can be attributed to the enhancement of chain flexibility and hydrogen bonds disruption in the solid electrolytes. When the amount of salt is increased, the values of  $D$ ,  $\mu$ , and  $n$  increase, resulting in a rise in conductivity.

Further understanding of the electrical properties of each electrolyte can be investigated using the electrical equivalent

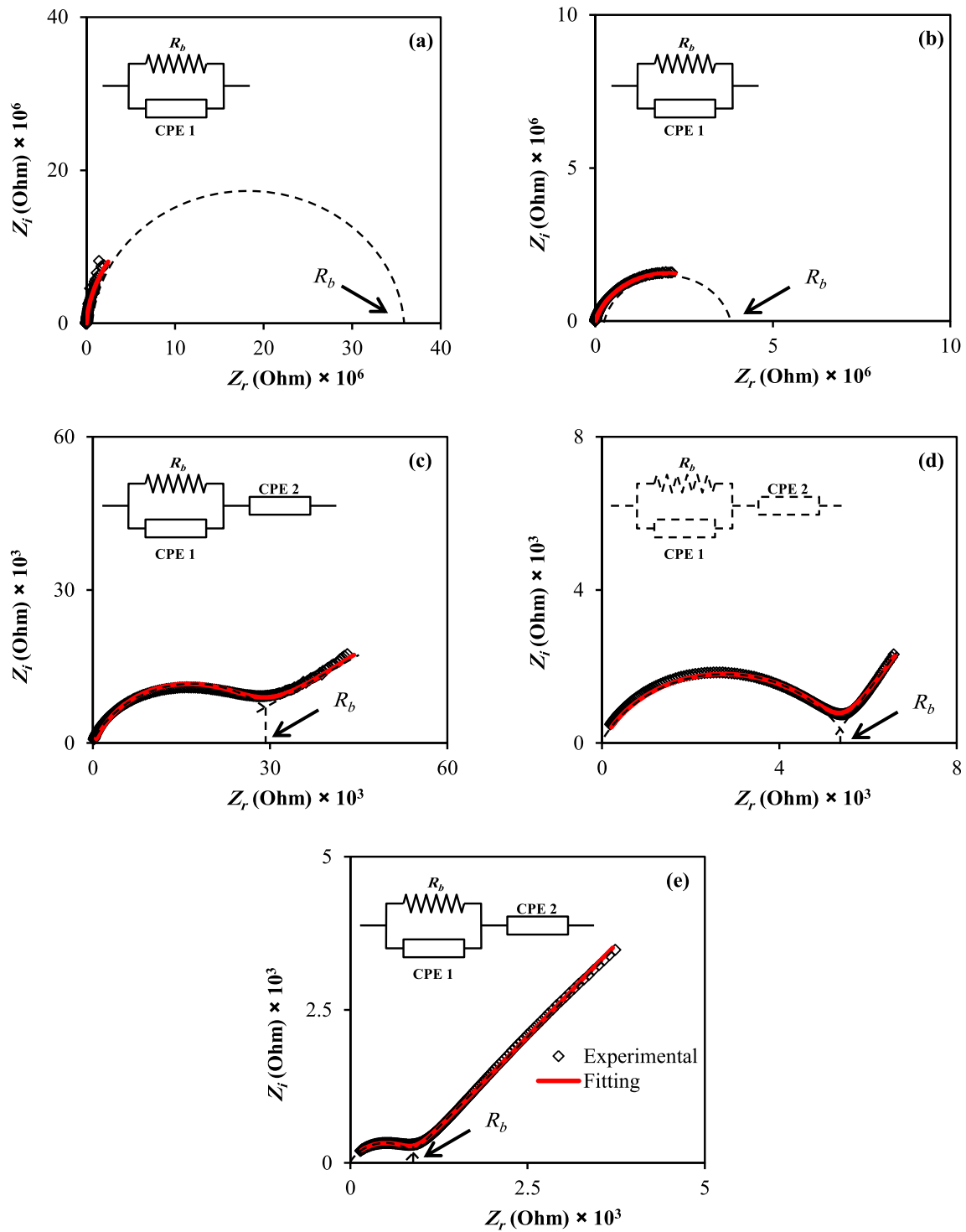


**Fig. 6** EIS plots for (a) PVMCNI1 (b), PVMCNI2 (c) PVMCNI3, (d) PVMCNI4, and (e) PVMCNI5 electrolyte films.

circuits (EECs) as shown in the impedance plots (Fig. 6). At high frequencies, the semicircle is a result of the parallel combination of bulk resistance ( $R_b$ ) and bulk capacitance, caused through ion migration and static (immobile) polymer chains. At lower frequencies, however, the sharp increase results from polarization at the electrode/electrolyte interfacial region from

the EECs modeling, the values of circuit elements can be identified where the expression of CPE impedance ( $Z_{CPE}$ ) as followed (Teo et al., (Kiel)0.2012.; Rani et al., 2020):

$$Z_{CPE} = \frac{1}{C\omega^p} \left[ \cos\left(\frac{\pi p}{2}\right) - i \sin\left(\frac{\pi p}{2}\right) \right] \quad (8)$$

**Table 5** The electrical parameters for PVA:MC:NaI systems at room temperature.

Sample	DC Conductivity (S/cm)	D (cm <sup>2</sup> /S)	$\mu$ (cm <sup>2</sup> .S /V)	N (cm <sup>-3</sup> )
PVMCNI1	$4.11 \times 10^{-10}$	–	–	–
PVMCNI2	$3.76 \times 10^{-9}$	–	–	–
PVMCNI3	$5.28 \times 10^{-7}$	$1.40 \times 10^{-8}$	$5.43 \times 10^{-7}$	$6.06 \times 10^{18}$
PVMCNI4	$2.78 \times 10^{-6}$	$2.10 \times 10^{-8}$	$8.18 \times 10^{-7}$	$2.12 \times 10^{19}$
PVMCNI5	$1.53 \times 10^{-5}$	$7.42 \times 10^{-8}$	$2.88 \times 10^{-6}$	$3.31 \times 10^{19}$

In Eq. (8),  $C$  and  $\omega$  represent the CPE capacitance and the angular frequency. At the same time,  $p$  is the deviation of the plot from the axis. The  $Z_r$  and  $Z_i$  of the impedance associated with the EEC are represented as:

$$Z_r = \frac{R_b^2 C \omega^p \cos\left(\frac{\pi p}{2}\right) + R_b}{2R_b C \omega^p \cos\left(\frac{\pi p}{2}\right) + R_b^2 C^2 \omega^{2p} + 1} \quad (9)$$

$$Z_i = \frac{R_b^2 C \omega^p \sin\left(\frac{\pi p}{2}\right)}{2R_b C \omega^p \cos\left(\frac{\pi p}{2}\right) + R_b^2 C^2 \omega^{2p} + 1} \quad (10)$$

The real impedance,  $Z_r$  and imaginary impedance,  $Z_i$  of the plots that consist of both spike and semicircle [PVMCNI1 and PVMCNI2] can be calculated using the equations below (Aziz et al., 2019):

$$Z_r = \frac{R_b^2 C_1 \omega^{p_1} \cos\left(\frac{\pi p_1}{2}\right) + R_b}{2R_b C_1 \omega^{p_1} \cos\left(\frac{\pi p_1}{2}\right) + R_b^2 C_1^2 \omega^{2p_1} + 1} + \frac{\cos\left(\frac{\pi p_2}{2}\right)}{C_2 \omega^{p_2}} \quad (11)$$

$$Z_i = \frac{R_b^2 C_1 \omega^{p_1} \sin\left(\frac{\pi p_1}{2}\right)}{2R_b C_1 \omega^{p_1} \cos\left(\frac{\pi p_1}{2}\right) + R_b^2 C_1^2 \omega^{2p_1} + 1} + \frac{\sin\left(\frac{\pi p_2}{2}\right)}{C_2 \omega^{p_2}} \quad (12)$$

where,  $p_1$  is the deviation semicircle from the vertical axis while  $p_2$  is the deviation of the spike from the horizontal axis. The high and low-frequency capacitance are designated as  $C_1$  and  $C_2$ , respectively. The EEC fitting parameters value for the PVA-MC-NaI systems are presented in Table 6. It is noticed that CPE2 values are increased with the increases of NaI concentration which explained the enhancement of the number of ions in the electrolytes, which increase the availability for electrode polarization, hence increasing the capacitance value at low frequency (Awasthi and Das, 2019). These also contribute to better mobility and dissociation of ions. This also verifies the formation of attractive forces between polymer chain segments and glycerol molecules, resulting in a lower cohesive attraction and an increase in the electrolyte's ionic conductivity (Khar et al., 2016; Yahya and Arof, 2003; Lee and Allcock, 2010). The PVMCNI5 solid electrolyte has shown to have the highest conductivity value.

Several formulae can be used to calculate the diffusion coefficient ( $D$ ), mobility ( $\mu$ ), and number density ( $n$ ) of ions using impedance data containing a spike (Arof et al., 2014; Yusof

et al., 2019). To begin, the following relationship is used to calculate  $D$  of ionic species:

$$D = D_0 \exp\{-0.0297[\ln D_0]^2 - 1.4348 \ln D_0 - 14.504\} \quad (13)$$

$$D_0 = \left( \frac{4k^2 l^2}{R_b^4 \omega_{min}^3} \right) \quad (14)$$

where,  $\omega_{min}$  is the angular frequency at the minimum  $Z_i$  value,  $l$  is the electrolyte thickness. By using Eq. (14) into Eq. (13), the  $D$  of the charge carriers is determined.

The following Eq. (15) is used to calculate the mobility ( $\mu$ ) of the ionic species,

$$\mu = \left( \frac{eD}{k_b T} \right) \quad (15)$$

where,  $T$  and  $k_b$  are the absolute temperature and Boltzmann constant, respectively.

Since the DC conductivity of ions is shown by,

$$\sigma_{dc} = ne\mu \quad (16)$$

Hence, Eq. (17) can be used to determine the density of ion carriers ( $n$ ).

$$n = \left( \frac{\sigma_{dc} K_b T \tau_2}{(e K_2 \epsilon_0 \epsilon_r A)^2} \right) \quad (17)$$

where  $\tau_2$  is the reciprocal of angular frequency corresponding to the minimum in  $Z_i$ ,  $K_2$  is the reciprocal of CPE2 as shown in Table 6.

### 3.4. Dielectric properties

The study of dielectric constants can be used to investigate and evaluate the conductivity nature of polymer electrolytes (Tamilselvi and Hema, 2016). The investigations of the dielectric permittivity and electric modulus will play a key role in understanding the ion transport mechanism, attributing to the presence of the dissociated salt, NaI, in PVA-MC based electrolyte films (Bharati et al., 2019; Hadi et al., 2020). The real part of dielectric permittivity ( $\epsilon'$ ) measures dipole alignment or polarization and is proportional to the capacitance. The imaginary part ( $\epsilon''$ ), on the other hand, is dielectric loss, which is related to conductance and reflects the energy needed for the alignment of the dipoles (Aziz et al., 2019). The study and detection of the development of neutral ion pairs formed from the association of dissolved ion pairs are of particular importance; as such formations can reduce the electrical conductivity (Aziz, 2016). As shown previously in XRD and FTIR studies, that increase of NaI quantity reduced the crystalline region. Thus, their impedance results showed that DC conductivity increased drastically. The real ( $\epsilon'$ ) and imaginary ( $\epsilon''$ ) parts of the dielectric permittivity (dielectric constant and

**Table 6** The EEC fitting parameters for PVMCNI systems at room temperature.

Sample	$p_1$	$p_2$	CPE <sub>1</sub>	CPE <sub>2</sub>
PVMCNI1	0.95	–	$1.25 \times 10^{-10}$	–
PVMCNI2	0.83	–	$5.88 \times 10^{-10}$	–
PVMCNI3	0.86	0.43	$1.67 \times 10^{-9}$	$1.75 \times 10^{-6}$
PVMCNI4	0.74	0.66	$1.11 \times 10^{-8}$	$3.57 \times 10^{-6}$
PVMCNI5	0.76	0.56	$1.43 \times 10^{-8}$	$4.03 \times 10^{-6}$

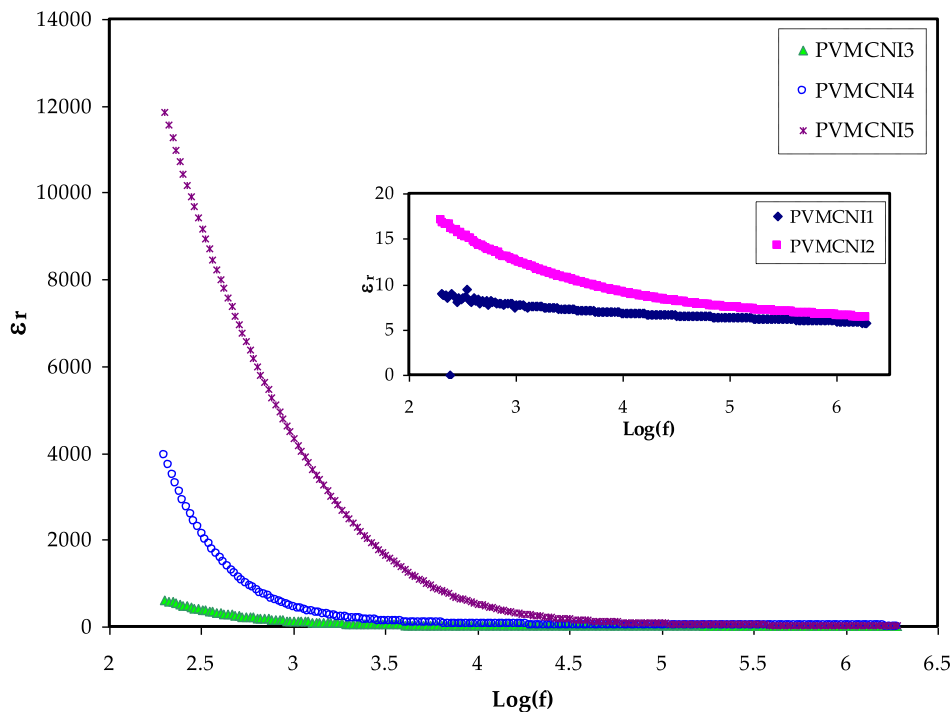


**Fig. 7** Dielectric constant versus log (f) for all electrolyte samples.

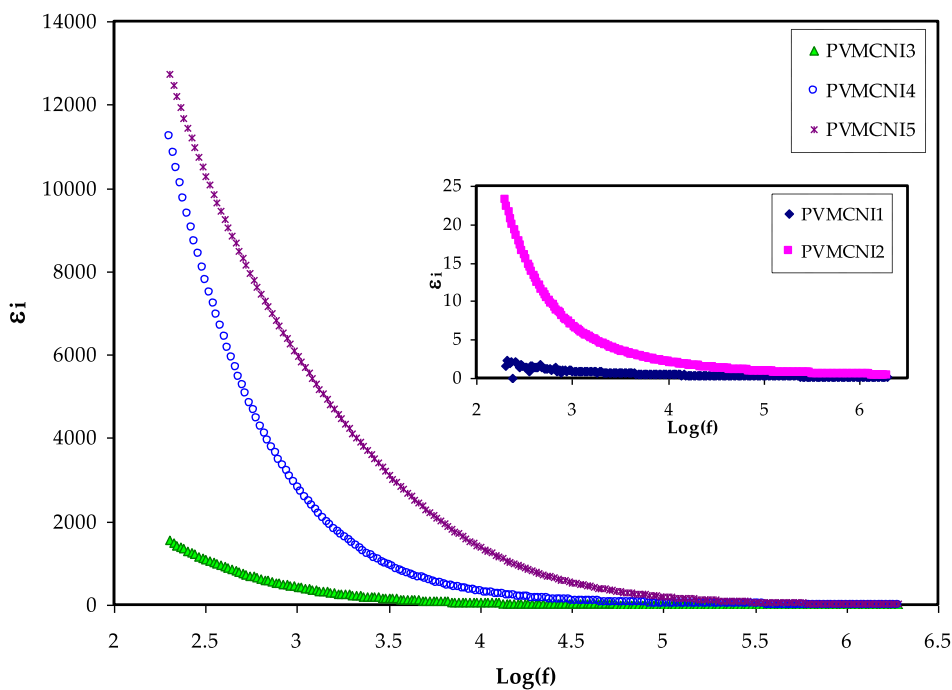


**Fig. 8** Dielectric loss versus log (f) for all electrolyte samples.

dielectric loss) were calculated from Eqs. (2) and (3). The dielectric constant and dielectric loss in the low-frequency region were found to be high, as shown in figures (7) and (8), which depict changes for the blend electrolyte samples.

This has resulted from the accumulation of charge carrier or the polarization of space charges at the electrode/electrolyte interface (Aziz et al., 2020; Teo et al., (Kiel)0.2012.; Bharati et al., 2019; Lokanatha Reddy et al., 2020). At a high

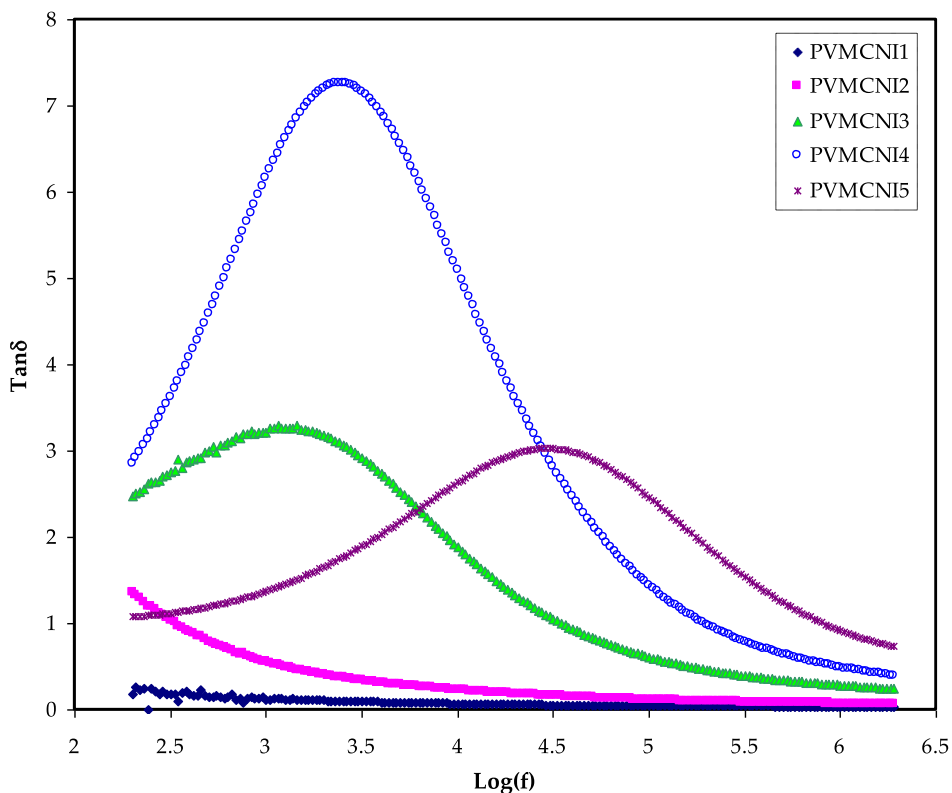


**Fig. 9** Loss tangent versus log (f) for all electrolyte samples.

frequency, this phenomenon lowers dielectric properties (i.e., the bulk property). In other words, reducing the applied electric field frequency increases the available drift time for charge carriers, which increases the dielectric constant and dielectric loss (Aziz et al., 2018). At high frequencies, the periodic reversal of the electric field occurs so quickly that no excess ion diffusion occurs in the field's direction and polarization reduces owing to the charge accumulation, causing the region to shrink and become frequency independent (Teo et al., (Kiel)0.2012). When compared to the other samples, the system incorporated with 50 wt% of NaI had the highest dielectric constant. This is due to the fact that amorphous regions in the system contribute significantly to both dielectric constant ( $\epsilon'$ ) and dielectric loss ( $\epsilon''$ ) (Awasthi and Das, 2019; Khair et al., 2016). The highest concentration of NaI salt has a large number of free charge carriers. Thus, due to the ions motion from one side to another, the electric potential of the surroundings will be perturbed (Bharati et al., 2019). The value of dielectric loss is more than the value of dielectric constant, as seen in the figures. This might be owing to the fact that the dielectric loss is affected by two contributions: the first is the dielectric polarization processes and the other is the DC conduction. Reddy et al. (Hadi et al., 2020) prepared PVA:NiS nano-composites using green approach. The authors showed that the dielectric constant of the nano-composites noticeably increased by loading NiS.

### 3.5. Tangent delta analysis

The loss tangent ( $\tan \delta$ ), also known as the dissipation factor, is the ratio of energy loss to energy stored in a periodical field

that may be determined using Eq. (4). The investigation of dielectric relaxation is essential to interpret the relaxation of dipoles in polymer electrolytes. As can be deduced from Fig. 9, the loss in the maximum tangent shifts to a higher frequency region as NaI concentration increases and approaches 50 wt%. The relaxation induced by the polarization of charge carriers existing in the material may mask the dielectric relaxation peaks due to permanent or induced dipoles in polymer electrolytes with considerable electrical conductivity (Hadi et al., 2020; Pritam and Sharma, 2019). Fig. 9 demonstrates the loss tangent varies with frequency for various solid polymer electrolytes. The single relaxation peak signature is a fingerprint of ionic conduction through polymer chain segmental motion (Arya and Sharma, 2018). The interpretation of the loss tangent shape can be based on Koops phenomenological model, whereby, assuming a homogeneous system, the negative slope of the low-frequency dispersion curve implied conduction dominated loss at lower frequencies through a parallel RC circuit. As a consequence, loss tangent grows with rising frequency, depicting a maximum at specific frequencies due to a more rapid rise of the active component (ohmic) than its reactive component (capacitive). Since the active component of the current is essentially (Ayesh, 2010; Morsi, 2019). At high frequencies, the loss tangent declines with the increase of frequency due to the independence of the active component of the current and the proportional rise of the reactive component with frequency. The broadness of the loss tangent peaks shows the presence of more than one relaxation process of the non-Debye type. These conclusions are supported by EEC fitting carried of impedance data, which showed that shifting the loss tangent relaxation peak towards a

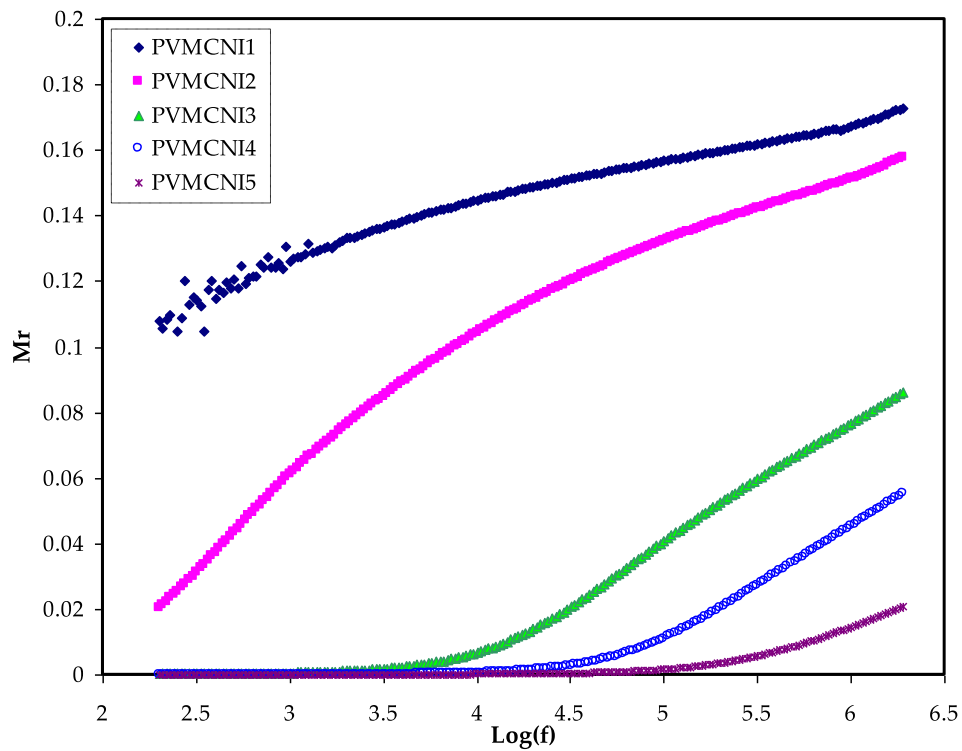


**Fig. 10** The real part of the electric modulus versus  $\log(f)$  for all electrolyte samples.

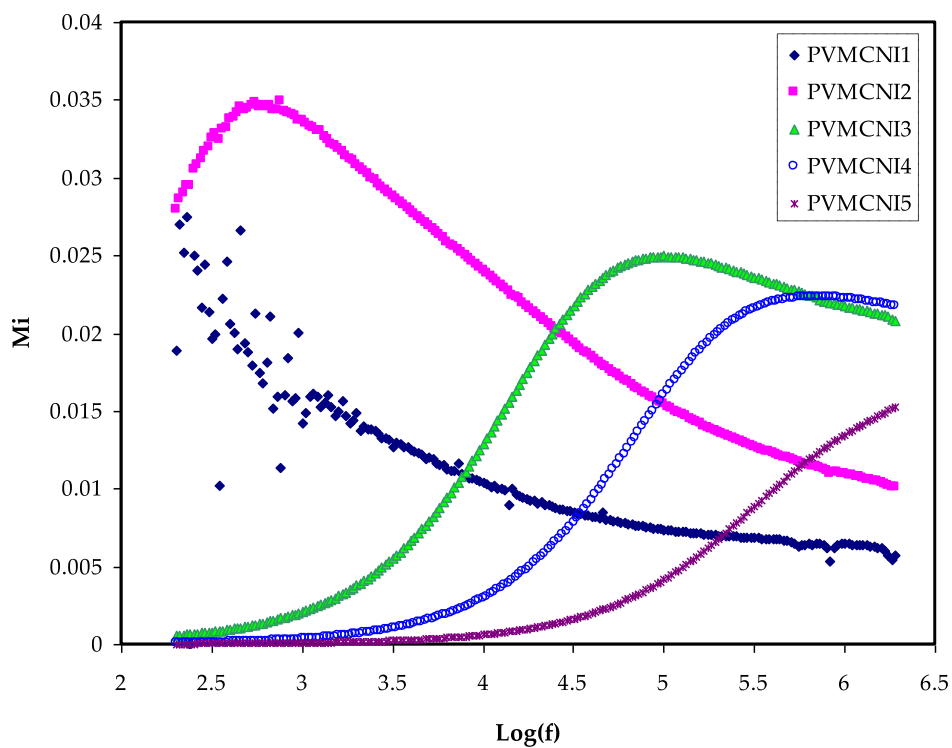


**Fig. 11** The imaginary part of the electric modulus versus  $\log(f)$  for all electrolyte samples.

high frequency side indicates the decrease of the relaxation time which is owed to faster ion dynamics. The breakdown of bond formation from the dipoles was shown to be reflected by an increase in peak intensity (Arya and Sharma, 2018; Ayes, 2010). Earlier studies have demonstrated the importance of estimating ion transport parameters, such as diffusion coefficient, carrier density and mobility. The relaxation time ( $\tau = 1/2\pi f_{\max}$ ), where  $f_{\max}$  is the relaxation frequency, can be determined using the single relaxation peak of  $\tan \delta$  spectra as shown in Fig. 9 (Kumar and Bhat, 2009).

From loss tangent and electric modulus plots, the broad nature of the peaks appeared in the  $\tan \delta$  and imaginary parts of the electric modulus, indicating the distribution of relaxation times.

The mentioned analysis of variation of different relaxation times is in agreement with the ionic conductivity value and follows the same trend. This exploration of various relaxation times and their correlation is sufficient to briefly explore the ion dynamics using the dielectric analysis. So, due to their var-

ious relaxation peak position a relaxation peak may be seen in one process and absent in another as in modulus spectra.

### 3.6. Modulus study

The comprehensive use of the modulus study allows a better understanding of the dielectric properties of the solid polymer electrolytes, particularly at low frequencies, by the transformation of the permittivity data into modulus data ( $M^* = j\omega CoZ^*$ ) using the Eqs. (5) and (6) (Rajendran et al., 2004).

From this converting, which deals to suppress the effects of electrode polarization at low frequency, it can investigate the conductivity relaxation. From the graph, it observes that for both types, there are two different regions corresponding to the high and low frequency. Figs. 10 and 11 show the variation of real ( $M_r$ ) and imaginary ( $M_i$ ) parts of electric modulus for the electrolyte films against frequency at ambient temperature.

As can be seen from the figures, both  $M_r$  and  $M_i$  increase as the frequency increase. Both  $M_r$  and  $M_i$  tend to have zero

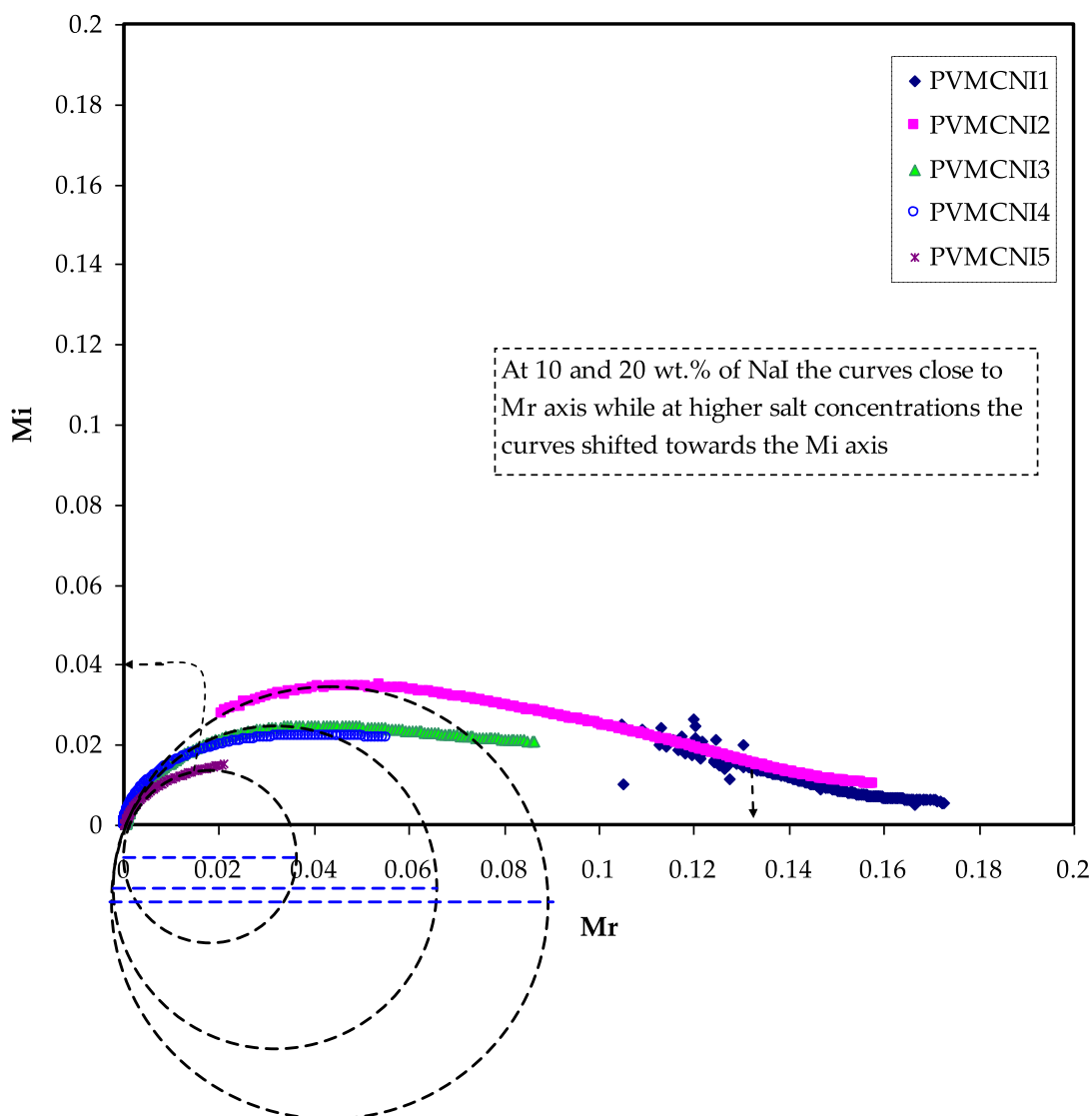


Fig. 12 Argand plot at ambient temperature for all the samples.

values with extended tails in low-frequency regions, implying that the polarization of electrodes, which induces charges to increase at stainless steel electrodes, is eliminated, and minimum participation is created. The large capacitance associated with the electrodes is mainly responsible for the formation of this long tail at low frequencies, confirming a non-Debye behaviour (Marf et al., 2020).

The  $M_r$  and  $M_i$  graphs, as illustrated in Figs. 10 and 11, indicate contrast (opposite) behaviour when compared to the  $\epsilon_r$  and  $\epsilon_i$  patterns. At the low-frequency range, large  $\epsilon_r$  and  $\epsilon_i$  values were seen (see Figs. 7 and 8). At the low-frequency region, the  $M_r$  and  $M_i$  point to the lowest values, indicating capacitive behaviour. Due to the addition of NaI in the polymer system, the modulus relaxation time ( $\tau_m$ ) was found to be reduced. The low value of relaxation time suggests that cations migrate quickly from one coordinating site of the host polymer to another, resulting in an increase in the ionic conductivity of solid polymer electrolyte. The value of  $M''$  is smaller at lower frequencies than at higher frequencies, which might be due to ion accumulation and, consequently, increased capacitance formation at the interfacial region.

As reported in previous work (Aziz and Abdullah, 2018; Aziz et al., 2019; Aziz et al., 2019; Aziz, 2018; Pradhan et al., 2008; Aziz et al., 2019), it has been documented that the relaxation time decreases as the ionic mobility and conductivity increases. It was discovered that the  $M_i$  spectra contains conductivity relaxation peaks, which moved to the higher frequency side with increasing NaI concentration in PVA:MC-based films. The concentration of NaI affects the mobility of charge carriers and the segmental motion of polymer chains. The appearance of peaks in the imaginary part ( $M_i$ ) spectra, indicates the existence and contribution of huge amounts of electrode polarization in the dielectric loss parameter which hidden the peaks in  $\epsilon_i$  spectra as a result of a couple of species motions, namely ionic and polymer segmental motions (Sengwa et al., 2008; Aziz, 2016). There is a directly proportional relationship between the relaxation time and salt concentration, which can be observed from the relaxation peak shifting to the lower frequency side with increasing the NaI salt concentration.

The Argand plot ( $M_i$ - $M_r$ ) for NaI-doped PVA:MC samples is shown in Fig. 12. The plots clearly reveal an incomplete half semicircle, indicating that the relaxation process is the non-Debye type (Mohomed et al., 2005). The non-Debye behaviour is owing to the fact that there are several types of polarization mechanisms in areal materials, as well as numerous interactions between ions and dipoles. As a result, a relaxation time distribution emerges. Furthermore, because of the reduction in resistivity, the  $M_i$ - $M_r$  curve deviates further from the semicircular arc as the NaI concentration increases, and the tail depresses more towards the  $M_i$  axis. This supported by the fact that the dielectric constant is significant at low frequencies (see Fig. 7). It was stated that if Argand's plot shows semicircular behaviour, relaxation is a result of the process of conductivity relaxation; otherwise, the relaxation is due to viscoelastic relaxation (or polymer molecular relaxation) (Sharma et al., 2013). In the Argand plots, depressed semicircles are a signature of deviation from ideal Debye behaviour. The intersection of plots with the real axis moves towards the origin as the concentration of NaI increases, showing an increase in mobility and, consequently, conductivity (Sharma et al., 2013). This coincides with the results of the XRD analysis. To distin-

guish between conductivity relaxation and viscoelastic relaxations, an understanding of the Argand plot is crucial. As the temperature increases, the  $Z_i$  and  $Z_r$  values decrease, causing the  $M_i$  and  $M_r$  values ( $M_i = \omega C_o Z_r, M_r = \omega C_o Z_i$ ) to deviate further towards the origin. Fig. 12 shows that the diameter of the semicircles is substantially below the real axis, revealing the relaxation time distribution. Ion transport takes place as a result of viscoelastic relaxation processes.

#### 4. Conclusions

In conclusion, the casting technique was used to prepare polymer blend electrolytes based on polyvinyl alcohol (PVA): Methyl Cellulose (MC) polymers incorporated with varied ratios of sodium iodide (NaI) salt. The structural and electrical behaviors of the prepared samples were studied through different characterization techniques. The amorphousness of the samples was determined by the presence of a broad hum in the XRD pattern. The semicrystalline behavior of the PVA and MC polymers is revealed by the XRD findings. The degree of crystallinity is reduced more efficiently with increasing the NaI due to the complexation between functional groups of the PVA:MC and the cations of the NaI salt. The interaction at the molecular level is evidenced by shifting peaks and variations in the strength of FTIR bands. The EIS technique has exhibited a highest ionic conductivity of  $1.53 \times 10^{-5}$  S/cm for a sample containing 50 wt% of NaI salt. To understand the whole electrical characteristics of the ion-conducting systems, the EIS results of each electrolyte were fitted with EECs.

The ion transport parameters, such as mobility, number density of carrier, and diffusion coefficient have found to be optimum for a highest conducting sample. The conductivity measurement was associated with the dielectric properties. At low frequencies, high dielectric constant and dielectric loss were observed. In terms of loss tangent and electric modulus plots, the relaxation behaviours of the samples are investigated.

#### Acknowledgments

We would like to acknowledge all support for this work by the University of Sulaimani, Charmo University and Komar University of Science and Technology.

#### References

- Pankaj Singh, Devesh Chandra Bharati, Horesh Kumar and A. L. Saroj, Ion transport mechanism and dielectric relaxation behavior of PVA-Imidazolium ionic liquid based polymer electrolytes, *Physica Scripta*
- Abdullah Zainab Waheed, 2019. Dong Yu, Biodegradable and Water Resistant Poly(vinyl) Alcohol (PVA)/Starch (ST)/Glycerol (GL)/Halloysite Nanotube (HNT) Nanocomposite Films for Sustainable Food Packaging. *Front. Mater.* 6, 58. <https://doi.org/10.3389/fmats.2019.00058>, ISSN = 2296-8016.
- Abiddin, J.F.B.Z., Ahmad, A.H., 2015. Fourier transform infrared spectroscopy and electrical characterization of methylcellulose based solid polymer electrolyte doped with sodium iodide *Jurnal Teknologi* 76 (3), 41–45.
- Agrawal, R.C., Pandey, G.P., 2008. Solid polymer electrolytes: materials designing and all-solid-state battery applications: an overview. *J Phys D Appl Phys.* 41 (22), 223001. <https://doi.org/10.1088/0022-3727/41/22/223001>.

- Arof, A.K., Amirudin, S., Yusof, S.Z., Noor, I.M., 2014. A method based on impedance spectroscopy to determine transport properties of polymer electrolytes. *PhysChemChemPhys* 16, 1856–1867.
- Arya, A., Sharma, A.L., 2017. Polymer electrolytes for lithium ion batteries: a critical study. *Ionics* 23, 497–540. <https://doi.org/10.1007/s11581-016-1908-6>.
- Arya, A., Sharma, A.L., 2018. Effect of salt concentration on dielectric properties of Lion conducting blend polymer electrolytes. *J Mater Sci: Mater Electron* 29, 17903–17920. <https://doi.org/10.1007/s10854-018-9905-3>.
- Awasthi, P.; Das, S. Reduced electrode polarization at electrode and analyte interface in impedance spectroscopy using carbon paste and paper. *Rev. Sci. Instrum.* 2019, 90, doi:10.1063/1.5123585.
- Ayesh, A.S., 2010. Electrical and optical characterization of PMMA doped with  $Y_{0.0025}Si_{0.025}Ba_{0.9725}(Ti_{0.9}Sn_{0.1})O_3$  ceramic. *Chinese J PolymSci* 28, 537–546.
- Aziz, S.B., 2016. Occurrence of electrical percolation threshold and observation of phase transition in chitosan  $(1-x):AgI_x$  ( $0.05 \leq x \leq 0.2$ )-based ion-conducting solid polymer composites. *Appl. Phys. A* 122, 706. <https://doi.org/10.1007/s00339-016-0235-0>.
- Aziz, S.B., 2016. Role of dielectric constant on ion transport: Reformulated Arrhenius equation. *Adv. Mater. Sci. Eng.* 2016.
- Aziz, S.B., 2018. The mixed contribution of ionic and electronic carriers to conductivity in chitosan based solid electrolytes mediated by CuNt salt. *J. Inorg. Organomet. Polym.* 28, 1942–1952.
- Aziz, S.B. et al, 2020. Fabrication of high performance energy storage EDLC device from proton conducting methylcellulose: dextran polymer blend electrolytes. *J. Mater. Res. Technol.* 9, 1137–1150.
- Aziz, S.B., Abdullah, O.G., Rasheed, M.A., Ahmed, H.M., 2017. Effect of High Salt Concentration (HSC) on Structural, Morphological, and Electrical Characteristics of Chitosan Based Solid Polymer Electrolytes. *Polymers* 9 (6), 187. <https://doi.org/10.3390/polym9060187>.
- Aziz, S.B., Abdullah, R.M., 2018. Crystalline and amorphous phase identification from the  $\tan\delta$  relaxation peaks and impedance plots in polymer blend electrolytes based on [CS: AgNt] x: PEO (x-1) ( $10 \leq x \leq 50$ ). *Electrochim. Acta* 285, 30–46.
- Aziz, Shujahadeen B, Brza, M.A., Mohamed, Pshko A, Kadir, M.F.Z., Hamsan, M.H., Abdulwahid, Rebar T, Woo, H.J., 2019. Increase of metallic silver nanoparticles in Chitosan: AgNt based polymer electrolytes incorporated with alumina filler. *Results Phys.* 13, 102326.
- Aziz, S.B., Kadir, M.F.Z., Hamsan, M.H. et al. Development of Polymer Blends Based on PVA:POZ with Low Dielectric Constant for Microelectronic Applications. *Sci Rep* 9, 13163 (2019). <https://doi.org/10.1038/s41598-019-49715-8>
- Aziz, S.B., Marif, B., R., Brza, M.A., Hamsan, M.H., Kadir, M.F.Z., 2019. Employing of Trukhan Model to Estimate Ion Transport Parameters in PVA Based Solid Polymer Electrolyte. *Polymers* 11, 1694.
- Aziz, S.B., Woo, T.J., Kadir, M.F.Z., Ahmed, H.M., 2018. A conceptual review on polymer electrolytes and ion transport models. *J Sci* 3, 1–17. <https://doi.org/10.1016/j.jsamd.2018.01.002>.
- Aziz, S.B., Karim, W.O., Brza, M.A., Abdulwahid, R.T., Saeed, S.R., Al-Zangana, S., Kadir, M.F.Z., 2019. Ion Transport Study in CS: POZ Based Polymer Membrane Electrolytes Using Trukhan Model. *Int. J. Mol. Sci.* 20, 5265.
- Aziz, S.B., Al-Zangana, S., Brza, M.A., Saeed, S.R., Abdulwahid, R. T., Kadir, M.F.Z., 2019. Study of Dielectric Properties and Ion Transport Parameters in Chitosan-Barium Nitrate Based Solid Polymer Electrolytes. *Int. J. Electrochem. Sci.* 14, 11580–11595.
- Aziz, S.B., Hamsan, M.H., Ranjdar, M., Abdullah, M.F.Z., Kadir, A., 2019. Promising polymer blend electrolytes based on chitosan: Methyl cellulose for EDLC application with high specific capacitance and energy density. *Molecules* 24, 2503.
- Aziz, S.B., Brza, M., Hamsan, M., Kadir, M., Muzakir, S., Abdulwahid, R.T., 2020. Effect of ohmic-drop on electrochemical performance of EDLC fabricated from PVA: Dextran: NH4I based polymer blend electrolytes. *J. Mater. Res. Technol.* 9, 3734–3745.
- Baker, M.I., Walsh, S.P., Schwartz, Z., Boyan, B.D., 2012. “A review of polyvinyl alcohol and its uses in cartilage and orthopedic applications” *Journal of Biomedical Materials Research Part B: Applied Biomaterials* 100B (5), 1451–1457.
- BalajiBhargav, P., Madhu Mohan, V., Sharma, A.K., Rao, V.V.R.N., 2007. Structural, electrical and optical characterization of pure and doped poly (vinyl alcohol) (PVA) polymer electrolyte films. *Int. J. Polym. Mater. Polym. Biomater.* 56 (6), 579–591.
- Basha, S., Rao, M.C., 2018.. Spectroscopic and Electrochemical Properties of [PVA/PVP] : [MgCl<sub>2</sub>H<sub>2</sub>O] Blend Polymer Electrolyte Films. *Int. J. Polym. Sci.*
- Bharati, D.C., Kumar, H., Saroj, A.L., 2019. Chitosan-PEG-NaI based bio-polymer electrolytes: Structural, thermal and ion dynamics studies. *Mater. Res. Express* 6. <https://doi.org/10.1088/2053-1591/ab66a3>.
- Brza, M.A., Aziz, Shujahadeen B., Anuar, H., Ali, Fathilah, Dannoun, Elham M.A., Saeed, Salah R., Mohammed, Sewara J., Abdulwahid, Rebar T., 2021. Green coordination chemistry as a novel approach to fabricate polymer: Cd (II)-complex composites: Structural and optical properties. *Opt. Mater.* 116, 111062.
- Choo, K., Ching, Y.C., Chuah, C.H., Julai, S., Liou, N.S., 2016 Jul 29. Preparation and Characterization of Polyvinyl Alcohol-Chitosan Composite Films Reinforced with Cellulose Nanofiber. *Materials (Basel)*. 9 (8), 644. <https://doi.org/10.3390/ma9080644>. PMID: 28773763; PMCID: PMC5509094.
- Daniel, R., S. Priscilla, S. Karthikeyan, S. Selvasekarapandian, S. Madeswaran and K. Sivaji. “Structural and Electrical Studies on PVP - Pan Blend Polymer System for Energy Storage Devices.” *International journal of current research and review* 10 (2018): 19-24. P22(4 of 6)
- Di Noto, V., Lavina, S., Giffin, G.A., Negro, E., Scrosati, B., 2011. Polymer electrolytes: Present, past and future. *ElectrochimicaActa* 57, 4–13.
- Fan, Xiayue et al, 2019. Investigation of the Environmental Stability of Poly(vinyl alcohol)-KOH Polymer Electrolytes for Flexible Zinc-Air Batteries. *Front. Chem.* 7(678), 22, Oct. <https://doi.org/10.3389/fchem.2019.00678>.
- Cun-dian Gao, Jun-li Ren, Shuai-yang Wang, Run-cang Sun, Li-hong Zhao, “Preparation of Polyvinyl Alcohol/Xylan Blending Films with 1,2,3,4-Butane Tetracarboxylic Acid as a New Plasticizer”, *Journal of Nanomaterials*, vol. 2014, ArticleID 764031, 8 pages, 2014. <https://doi.org/10.1155/2014/764031>
- Hadi, J.M., Aziz, S.B., Saeed, S.R., Brza, M.A., Abdulwahid, R.T., Hamsan, M.H., Abdullah, R.M., Kadir, M.F.Z., Muzakir, S.K., 2020. Investigation of ion transport parameters and electrochemical performance of plasticized biocompatible chitosan-based proton conducting polymer composite electrolytes. *Membranes (Basel)*. 10, 1–27. <https://doi.org/10.3390/membranes10110363>.
- Hadi, J.M., Aziz, S.B., Mustafa, M.S., Hamsan, M.H., Abdulwahid, R.T., Kadir, M.F.Z., Ghareeb, H.O., 2020. Role of nano-capacitor on dielectric constant enhancement in PEO:NH<sub>4</sub>SCN:xCeO<sub>2</sub> polymer nano-composites: Electrical and electrochemical properties. *J. Mater. Res. Technol.* 9, 9283–9294. <https://doi.org/10.1016/j.jmrt.2020.06.022>.
- Hadi, J.M., Aziz, S.B., Mustafa, M.S., Brza, M.A., Hamsan, M.H., Kadir, M.F.Z., Ghareeb, H.O., Hussein, S.A., 2020. Electrochemical impedance study of proton conducting polymer electrolytes based on PVC doped with thiocyanate and plasticized with glycerol. *Int. J. Electrochem. Sci.* 15, 4671–4683 <https://doi.org/10.20964/2020.05.34>.
- Ibrahim, S., Yasin, S.M.M., Nee, N.M., et al, 2012. Conductivity and dielectric behavior of PVA based solid nanocomposite polymer electrolytes. *Solid State Commun* 152, 426–434.
- Jaipal Reddy, M., Chu, P.P., 2002. Ion pair formation and its effect in PEO: Mg solid polymer electrolyte system. *J. Power Sources* 109 (2), 340–346. [https://doi.org/10.1016/s0378-7753\(02\)00084-8](https://doi.org/10.1016/s0378-7753(02)00084-8).

- Jiang, L., Yang, T., Peng, L., Dan, Y., 2015. Acrylamide modified poly (vinyl alcohol): Crystalline and enhanced water solubility. *RSC Adv.* 5, 86598–86605.
- Khiar, A.S.A., Anuar, M.R.S., Parid, Md., M.A., 2016. Effect of 1-ethyl-3-methylimidazolium nitrate on the electrical properties of starch/chitosan blend polymer electrolyte. *Mater. Sci. Forum* 846, 510–516. <https://doi.org/10.4028/www.scientific.net/MSF.846.510>.
- Kim, B.K., Sy, S., Yu, A. and Zhang, J. (2015). Electrochemical Supercapacitors for Energy Storage and Conversion. In *Handbook of Clean Energy Systems*, J. Yan
- Kotobuki, M. (2020). Polymer Electrolytes. In *Polymer Electrolytes* (eds T. Winie, A.K. Arof and S.Thomas). <https://doi.org/10.1002/9783527805457.ch1.P5> (20 of 417)
- Kumar, M.S., Bhat, D.K., 2009. LiClO<sub>4</sub>-doped plasticized chitosan as biodegradable polymer gel electrolyte for supercapacitors. *J. Appl. Polym. Sci.* 114, 2445–2454. <https://doi.org/10.1002/app.30716>.
- Lee, D.K., Allcock, H.R., 2010. The effects of cations and anions on the ionic conductivity of poly[bis(2-(2-methoxyethoxy)ethoxy) phosphazene] doped with lithium and magnesium salts of trifluoromethanesulfonate and bis(trifluoromethanesulfonyl)imide. *Solid State Ionics* 181, 1721–1726. <https://doi.org/10.1016/j.ssi.2010.09.051>.
- Liu, J., Wang, J., Xu, C., Jiang, H., Li, C., Zhang, L., Lin, J., Shen, Z. X., 2017 Nov 15. *Advanced Energy Storage Devices: Basic Principles, Analytical Methods, and Rational Materials Design.* *AdvSci (Weinh).* 5 (1), 1700322. <https://doi.org/10.1002/advs.201700322>.
- Lokanatha Reddy, P., Deshmukh, Kalim, Kovářik, Tomáš, David Reiger, N., Nambiraj, Arunai, Lakshmi pathy, R., Khadheer Pasha, S.K., 2020. Enhanced dielectric properties of green synthesized Nickel Sulphide (NiS) nanoparticles integrated polyvinylalcohol nanocomposites. *Mater. Res. Express* 7, 064007.
- Malhotra, B., Keshwani, A., Kharkwal, H., 2015. Natural polymer based cling films for food packaging. *Int. J. Pharm. Pharm. Sci.* 7, 10–18.
- Marf, A.S., Abdullah, R.M., Aziz, S.B., 2020. Structural, Morphological, Electrical and Electrochemical Properties of PVA:CS-Based Proton-Conducting Polymer Blend Electrolytes. *Membranes* 10, 71.
- Mohomed, K., Gerasimov, T.G., Moussy, F., Harmon, J.P., 2005. A broad spectrum analysis of the dielectric properties of poly(2-hydroxyethyl methacrylate). *Polymer* 46, 3847–3855.
- Morsi, M. et al, 2019. Preparation, structural analysis, morphological investigation and electrical properties of gold nanoparticles filled polyvinyl alcohol/carboxymethyl cellulose blend. *J Mater Res Technol.* <https://doi.org/10.1016/j.jmrt.2019.09.07>.
- Negim, E. et al, 2014. Improving biodegradability of polyvinyl alcohol/starch blend films for packaging applications. *International Journal of Basic and Applied Sciences* 3, 263–273.
- Ngai, K.S., Ramesh, S., Ramesh, K., Juan, J.C., 2016. A review of polymer electrolytes: fundamental, approaches and applications. *Ionics* 22 (8), 1259–1279. <https://doi.org/10.1007/s11581-016-1756-4>.
- Olewnik-Kruszkowska, Ewa et al. “Antibacterial Films Based on PVA and PVA-Chitosan Modified with Poly(Hexamethylene Guanidine).” *Polymers* vol. 11,12 2093. 13 Dec. 2019, doi:10.3390/polym11122093
- OmedGh. Abdullah, Shujahadeen B. Aziz, Mariwan A. Rasheed, Structural and optical characterization of PVA:KMnO<sub>4</sub> based solid polymer electrolyte, *Results in Physics*, Volume 6,2016, Pages 1103-1108, ISSN 2211-3797, <https://doi.org/10.1016/j.rinp.2016.11.050>.
- Pan, Y., Xu, K., Wu, C., 2019. Recent progress in supercapacitors based on the advanced carbon electrodes. *Nanotechnology Reviews* 8 (Issue 1), 299–314. <https://doi.org/10.1515/ntrev-2019-0029>.
- Park, J.S., Park, J.W., 2001. Ruckenstein, E, Thermal and dynamic mechanical analyses of PVA/MC blend hydrogels. *Polymer* 42, 4271–4280.
- Polu, A.R., Kumar, R., 2013. Preparation and characterization of pva based solid polymer electrolytes for electrochemical cell applications. *Chin J PolymSci* 31 (4), 641–648. <https://doi.org/10.1007/s10118-013-1246-3>.
- Pradhan, D.K., Choudhary, R.N.P., Samantaray, B.K., 2008. Studies of Dielectric Relaxation and AC Conductivity Behavior of Plasticized Polymer Nanocomposite Electrolytes. *Int. J. Electrochem. Sci.* 3, 597–608.
- Pritam, Arya, A., & Sharma, A, 2019. Dielectric relaxations and transport properties parameter analysis of novel blended solid polymer electrolyte for sodium-ion rechargeable batteries. *J. Mater. Sci.* 54, 7131–7155. <https://doi.org/10.1007/s10853-019-03381-3>.
- Rajendran, S., Sivakumar, M., Subadevi, R., 2004. Investigations on the effect of various plasticizers in PVA–PMMA solid polymer blend electrolytes. *Mater. Lett.* 58, 641–649.
- Rani, P., Ahamed, M.B., Deshmukh, K., 2020. Dielectric and electromagnetic interference shielding properties of carbon black nanoparticles reinforced PVA/PEG blend nanocomposite films. *Mater. Res. Express* 7 (6), 064008. <https://doi.org/10.1088/2053-1591/ab9853>.
- Rani, P., Ahamed, M.B., Deshmukh, K., 2021. Structural, dielectric and EMI shielding properties of polyvinyl alcohol/chitosan blend nanocomposites integrated with graphite oxide and nickel oxide nanofillers. *J. Mater. Sci.: Mater. Electron.* 32 (1), 764–779. <https://doi.org/10.1007/s10854-020-04855-w>.
- Rani, P., Ahamed, B., & Deshmukh, K. (2020). Electromagnetic interference shielding properties of graphene quantum-dots reinforced poly(vinyl alcohol)/polypyrrole blend nanocomposites. *Journal of Applied Polymer Science*, 49392. doi:10.1002/app.49392
- Rani, N.S., Sannappa, J., Demappa, T., et al, 2014. Structural, thermal, and electrical studies of sodium iodide (NaI)-doped hydroxypropyl methylcellulose (HPMC) polymer electrolyte films. *Ionics* 20, 201–207. <https://doi.org/10.1007/s11581-013-0952-8>.
- Rina Afiani Rebia, Sélène Rozet, Yasushi Tamada, Toshihisa Tanaka, Biodegradable PHBH/PVA blend nanofibers: Fabrication, characterization, in vitro degradation, and in vitro biocompatibility, *Polymer Degradation and Stability*, Volume 154,2018,Pages 124-136, ISSN 0141-3910, <https://doi.org/10.1016/j.polymdegradstab.2018.05.018>.
- Reddy, P. Lokanatha, Deshmukh, Kalim, Chidambaram, K., Ali, Mohammad M. Nazeer, Sadasivuni, Kishor Kumar, Kumar, Y. Ravi, Lakshmi pathy, R., Pasha, S. K. Khadheer, 2019. Dielectric properties of polyvinyl alcohol (PVA) nanocomposites filled with green synthesized zinc sulphide (ZnS) nanoparticles. *J. Mater. Sci.: Mater. Electron.* 30 (5), 4676–4687. <https://doi.org/10.1007/s10854-019-00761-y>.
- Reddy, Peram Lokanatha, Deshmukh, Kalim, Kovářik, Tomáš, Nambiraj, Narayanasamy Arunai, Shaik, Khadheer Pasha, 2020. Green chemistry mediated synthesis of cadmium sulphide/polyvinyl alcohol nanocomposites: Assessment of microstructural, thermal, and dielectric properties. *Polym. Compos.* 41 (5), 2054–2067. <https://doi.org/10.1002/pc.v41.510.1002/pc.25520>.
- Remiš, T., Bělský, P., Kovářik, T., Kadlec, J., Ghafouri Azar, M., Medlín, R., Vavruňková, V., Deshmukh, K., Sadasivuni, K.K., 2021. Petr Belský, Tomáš Kovářik, Jaroslav Kadlec, Mína Ghafouri Azar, Rostislav Medlín, Veronika Vavruňková, Kalim Deshmukh and Kishor Kumar Sadasivuni, Study on Structure, Thermal Behavior, and Viscoelastic Properties of Nanodiamond-Reinforced Poly (vinyl alcohol) Nanocomposites. *Polymers* 13 (9), 1426. <https://doi.org/10.3390/polym13091426>.
- Rozali, M.I.H., Samsudin, A.S., Isa, M.I.N., 2012. Ion conducting mechanism of carboxy methylcellulose doped with ionic dopant salicylic acid based solid polymer electrolytes. *Int J ApplSciTechnol* 2, 113–121.
- Saeed, M.A.M., Abdullah, O.G., 2020. Effect of High Ammonium Salt Concentration and Temperature on the Structure, Morphology, and Ionic Conductivity of Proton-Conductor Solid Polymer Electrolytes Based PVA. *Membranes*. 10 (10), 262. <https://doi.org/10.3390/membranes10100262>.

- Saito, M., Kawaharasaki, S., Ito, K., Yamada, S., Hayamizu, K., Seki, S., 2017. Strategies for fast ion transport in electrochemical capacitor electrolytes from diffusion coefficients, ionic conductivity, viscosity, density and interaction energies based on HSAB theory. *RSC. Advances* 7 (24), 14528–14535. <https://doi.org/10.1039/C7RA00455A>.
- Sengwa, R.J., Choudhary, S., Sankhla, S., 2008. Low frequency dielectric relaxation processes and ionic conductivity of montmorillonite clay nanoparticles colloidal suspension in poly(vinyl pyrrolidone)-ethylene glycol blends. *Express Polym. Lett.* 2, 800–809.
- Senna, M., Helal, R., Mostafa, T., El-Naggar, A. (2018). 'Thermal Decomposition Properties of Gamma-Irradiated Polyvinyl Alcohol (PVA)/Methyl Cellulose (MC) Blends', The International Conference on Chemical and Environmental Engineering, 9(9th International Conference on Chemical & Environmental Engineering), pp. 339-357. doi: 10.21608/iccee. 2018.34676
- Sharma, P., Kanchan, D.K., Gondaliya, N., Pant, M., Jayswal, M.S., 2013. Conductivity relaxation in Ag<sup>+</sup> ion conducting PEO-PMMA-PEG polymer blends. *Ionics* 19, 301–307.
- Singh, P., Saroj, A.L., 2020. Effect of SiO<sub>2</sub> Nano-particles on Plasticized Polymer Blend Electrolytes: Vibrational, Thermal, and Ionic Conductivity Study. *Polymer-Plastics Technology and Materials* 1–8. <https://doi.org/10.1080/25740881.2020.1793202>.
- Singh, P., Bharati, C.D., Gupta, P.N., Saroj, A.L., 2018. Vibrational, thermal and ion transport properties of PVA-PVP-PEG-MeSO<sub>4</sub>Na based polymer blend electrolyte films. *J Non-Cryst Solids* 494, 21–30.
- Sugantha Kumari, V., Khaleel Basha, S., Sudha, P.N., 2012. Physicochemical and morphological evaluation of chitosan/poly(vinyl alcohol)/methylcellulose chemically cross-linked ternary blends. *Polym. Bull.* 68 (5), 1387–1393. <https://doi.org/10.1007/s00289-011-0645-2>.
- Tamilselvi, P., Hema, M., 2016. Structural, thermal, vibrational, and electrochemical behavior of lithium ion conducting solid polymer electrolyte based on poly(vinyl alcohol)/poly(vinylidene fluoride) blend. *Polym. Sci. Ser. A* 58, 776–784. <https://doi.org/10.1134/S0965545X16050199>.
- Tănase, E.E., Popa, M.E., Rapa, M., OvidiuPopa, 2015. Preparation and Characterization of Biopolymer Blends Based on Polyvinyl Alcohol and Starch. *Romanian Biotechnological Letters* 20 (20), 10306–10315.
- Tanase, E.E., Rapa, M., Popa, S., 2014. Biopolymers based on renewable resources—A review. *Sci. Bull. Ser. F Biotechnol.* 18, 188–195.
- Teo, L.P., Buraidah, M.H., Nor, A.F.M., Majid, S.R., . Conductivity and dielectric studies of Li 2SnO 3. *Ionics* 18, 655–665. <https://doi.org/10.1007/s11581-012-0667-2>.
- Tretinnikov, O.N., Zagorskaya, S.A., 2012. Determination of the degree of crystallinity of poly(vinyl alcohol) by FTIR spectroscopy. *J. Appl. Spectrosc.* 79 (4), 521–526.
- Wang, Y., Song, Y., Xia, Y., 2016. Electrochemical capacitors: Mechanism, materials, systems, characterization and applications. *Chem. Soc. Rev.* 45, 5925–5950.
- Wani, S.I., Rafiuddin, R., 2018. Impedance spectroscopy and conductivity studies of KCl-doped solid electrolyte. *J TheorApplPhys* 12, 141–146. <https://doi.org/10.1007/s40094-018-0294>.
- Yahya, M.Z.A., Arof, A.K., 2003. Effect of oleic acid plasticizer on chitosan-lithium acetate solid polymer electrolytes. *Eur. Polym. J.* 39, 897–902. [https://doi.org/10.1016/S0014-3057\(02\)00355-5](https://doi.org/10.1016/S0014-3057(02)00355-5).
- Yao, P., Yu, H., Ding, Z., Liu, Y., Lu, J., Lavorgna, M., Wu, J., Liu, X., 2019. Review on Polymer-Based Composite Electrolytes for Lithium Batteries. *Front. Chem.* 7, 522. <https://doi.org/10.3389/fchem.2019.00522>.
- Yusof, Y.M., Shukur, M.F., Hamsan, M.H., Jumbri, K., Kadir, M.F. Z., 2019. Plasticized solid polymer electrolyte based on natural polymer blend incorporated with lithium perchlorate for electrical double-layer capacitor fabrication. *Ionics*. <https://doi.org/10.1007/s11581-019-03096-0>.
- Marco Zeiger, Simon Fleischmann, Benjamin Krüner, Aura Tolosa, Stephan Bechtel, Mathias Baltes, AnnaSchreiber, RikoMoroni, SeverinVierrath, Simon Thiele, Volker Presser. Influence of carbon substrate on the electrochemical performance of carbon/manganese oxide hybrids in aqueous and organic electrolytes. *RSC Advances* 2016, 6 (109) , 107163-107179. <https://doi.org/10.1039/C6RA24181F>
- Zhong, Cheng, Yida Deng, Wen-bin Hu, JinliQiao, Lei Zhang and J. Zhang. "A review of electrolyte materials and compositions for electrochemical supercapacitors." *Chemical Society reviews* 44 21 (2015): 7484-539 . p11 (9 of 58)
- Zhu, Guoquan, Wang, Fagang, Xu, Kejing, Gao, Qiaochun, & Liu, Yuying. (2013). Study on properties of poly(vinyl alcohol)/polyacrylonitrile blend film. *Polimeros*, 23(2), 146-151. Epub April 16, 2013. <https://doi.org/10.4322/polimeros.2013.076>.